A Dual-Mode Ultra-Wideband Wireless Platform for Remote Patient Monitoring Systems

A feasibility study

AALBORG UNIVERSITET

Master Thesis
Spring Semester 2012
School of Information and Communication Technology (SICT)
Study board for Electronics and IT

Project group: RISC10
Sergi Bisbe
Carlos Reyes

AALBORG UNIVERSITET

Study board for Electronics and IT
Fredrik Bajers Vej 5
Telephone: (+45) 9940 9940
http://www.sict.aau.dk/

Title:
A Dual-Mode Ultra-Wideband Wireless Platform for Remote Patient Monitoring Systems.

Project period:
15/2/2012 – 30/5/2012
Spring semester 2012

Project group:
RISC10

Group members:
Sergi Bisbe Novoa
Carlos Reyes Navarro

Supervisors:
Ming Shen
Jan H. Mikkelsen

Copies: 3

Number of pages: 76

Finished: 30/5/2012

Abstract:

The combination of two factors demands the need to find a solution that guarantees the well-being of the people suffering from chronic diseases. On the one hand, the increase of the life expectancy leads to an older world's population. On the other hand, the aged are more likely to suffer from chronic diseases and/or injuries.

This thesis deals with the design of an Ultra-Wideband-based node of a Remote Patient Monitoring (RPM) network. This node must be able to measure, collect and transmit some medical parameters of a patient. Existing RPM networks use two different hardware platforms: one for measuring and another one for transmitting. This leads to high cost and high power consumption. Since a RPM network is typically composed by hundreds or thousands of nodes, a new platform with lower cost and power consumption is vital to make such a system work. This thesis explores the viability to achieve the dual-mode operation: Radar Mode (RM) to obtain a certain parameter and Data Transmission Mode (DTM) to send it to another node.

A platform using Impulse-Radio Ultra-Wideband (IR-UWB) has been proposed to accomplish this goal. The simulations done verified its feasibility. Moreover, the physical experiments carried out validated the transmitter. Nevertheless, due to time and hardware limitations, the receiver has not been experimentally validated yet.

AALBORG UNIVERSITET

Study board for Electronics and IT
Fredrik Bajers Vej 5
Telephone: (+45) 9940 9940
http://www.sict.aau.dk/

Titel:
En dual-mode platform til trådløs patient monitorering, baseret på ultra bredbånds teknlogi

Projektperiode:
15/2/2012 – 30/5/2012
Forårssemesteret 2012

Projektgruppe:
RISC10

Gruppemedlemmer:
Sergi Bisbe Novoa
Carlos Reyes Navarro

Vejleder:
Ming Shen
Jan H. Mikkelsen

Oplagstal: 3

Sidetal: 76

Afsluttet den: 30/5/2012

Synopsis:

Antallet af kroniske sygdomme hos folk, stiger i takt med deres alder. Dette kombineret med en øget forventet levetid stiller store krav til sundhedsvæsnet. Det er derfor nødvendigt med teknologiske hjælpesystemer til sikring af livskvalitet hos de ældre.

Denne rapport tager udgangspunkt i trådløs patient monitorering (RPM), som en potentiel løsning på udfordringen med sikring af livskvalitet. Et sådan RPM system skal være i stand til at måle, behandle og transmittere forskellige helbredsparametre for en patient. Eksisterende RPM systemer er baseret på to forskellige hardware platforme, hvor den ene forestår måling og behandling af data, mens den anden platform forestår transmitteringen af de samme data. Dette medfører en forhøjet pris samt et øget strømorbrug. Et fuldt udbygget RPM system vil typisk bestå af hundrede eller tusinde enheder, og derfor vil en ny, billigere og mere energieffektiv, platform være særdeles vigtig.

I denne rapport tages der udgangspunkt i en ultra bredbåndsteknologi, der gør det muligt at implementere måle, behandle og transmitteringselementerne i en og samme hardware platform. Disse funktioner opdeles i rapporten i to elementer; Radar-mode (RM) der forestår dataindsamlingen og sender-mode (DTM) der forestår datatransmissionen. Platformen benytter en ultra-bredbåndsteknologi baseret på ganske korte pulser. Den foreslåede platform er i sin helhed verificeret gennem simuleringe, og desuden er senderdelen verificeret gennem målinger. Grundet hardware begrænsninger har det dog ikke været muligt at teste modtagerdelen eksperimentelt inden rapportaflevering.

Preface

This document presents a Master's Thesis work done by Carlos Reyes and Sergi Bisbe in Aalborg University during spring semester of 2012.

This thesis deals with the design of a Dual-Mode Ultra-Wideband-based node of a Remote Patient Monitoring (RPM) network. The document is organized as follows:

Chapter 1 provides a general view of the Thesis, explaining the background, motivation, past related work, objectives and methodology. The chapter also explains a system description and the development tools. .

Chapter 2 introduces the Remote Patient Monitoring Systems and an analysis of the state of the art of this kind of systems.

Chapter 3 starts with an overview of Ultra-Wideband technology. The aim is to understand the selection of UWB among other wireless technologies. In the chapter, the choice of Impulse Radio UWB is also explained.

Chapter 4 describes the different parts of the system, transmitter, channel and receiver. The system simulated results and the experimental results of the transmitter are also shown.

Finally, Chapter 5 carries out with the conclusions of the thesis.

It should be noted that receiver has not been verified with experimental results for lack of time and hardware resources.

Sergi Bisbe

Carlos Reyes

To our family and friends.

A particular acknowledgement for Ming and Jan.

TABLE OF CONTENTS

CHAPTER 1. INTRODUCTION

1.1. Background and motivation

Chronic diseases are responsible for the 63% of the deaths in the world [1]. These are usually long duration and slow progression diseases and many deaths, due to them, could be reduced with an improved health care system.

Among all the people suffering from chronic diseases, there is a particularly affected group: the elderly. For instance, in the Fig 1.1, it is seen that chronic diseases cause most of the deaths among the older Americans. Besides that, the world's population is ageing. According to the United Nations Population Fund [2], the number of people aged 60 years or older is expected to triple during the next 45 years; composing the 21% of the population by 2050. The combination of these two facts makes evident the need for improving the current health systems so they can cope with the future demand in terms of chronic patients' caregiving.

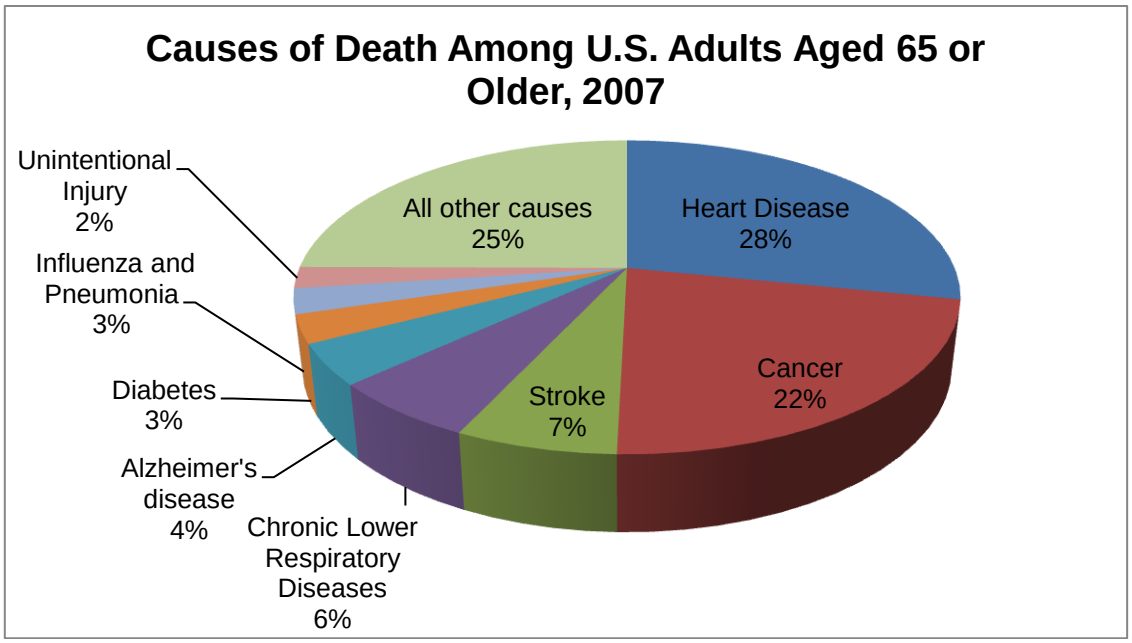

Fig.1. 1.Causes of death among U.S adults aged 65 or older, 2007

[Source: CDC, National Center for Health Statistics, National Vital Statistics System, 2007]

.

There are many ways to contribute to this improvement; one of them is known as Remote Patient Monitoring (RPM). Chronic patients need monitoring. Monitoring means to check and evaluate a certain phenomenon of the body. Until recently, this task required the presence of the patient in the hospital or the primary care center and a doctor or a nurse to carry it out. However, RPM allows changing this situation. With a RPM system, the checking can be done

wherever the patient is and the doctor will be able to evaluate the data remotely and will receive a notification if something goes wrong.

The type of RPM system is different for each monitored phenomena, i.e. for each chronic disease. This thesis deals with the ones that can be measured without contact. In this group are included most of the death causes in Fig. 1.1 such as heart and respiratory diseases, cancers, strokes and even unintentional injuries as falls. In these cases, the RPM system monitors the particular medical phenomenon like the hearth and/or respiratory rates, a tumor or the movement of the patient. The system is able to collect, process and transmit the data so the parameters are recorded and processed and an alarm can be triggered if necessary.

The implementation of RPM systems, at home, mobile devices and hospitals, will have repercussions in patients, health professionals and health systems. The well-being of the patients will be improved. On the one hand the system can save their lives or prevent irreversible damages by means of its quick response. On the other hand, it spares them the need to go to the hospital or even saves them any inconvenience by measuring the parameters without their concern. The health professionals will also benefit. RPM systems will keep them from wasting their time in routine procedures thus they can work in what really matters and where they are needed to. Finally, the social health and welfare will be able to reduce expenses and to optimize the cares given by avoiding unnecessary hospitalizations, reducing the burden on caregivers and giving the citizens a better quality of life [3]. The FCC in its National Broadband Plan estimates that RPM can generate net savings of $197 billion over the next 25 years in the U.S.

1.2. Past related work, challenges and objectives

The interest in RPM has increased during the last years. Since the sustainability of the face-to-face health model is threatened by the forecasts, the research in RPM has attracted many researchers and companies. Large companies such as Bosch, Phillips, Honeywell or Intel already have comercial RPM devices as the Health Buddy, Telestation, Genesis DM and Health Guide PHS6000 respectively. Nevertheless, these are just the tip of the iceberg. There are hundreds of smaller companies offering RPM solutions. Apart from private businesses, there is also lots of research in Universities [4]. A summary of the in-depth analysis carried out can be read in the second chapter.

Despite the work done, there is still much room for improvement. An RPM system must be robust, reliable and safe. It also must have a low cost in terms of manufacturing and operation, which implies keeping the power consumption as low as possible. The maximum transparence to the user is another positive characteristic. That means that the patience must barely notice that the system is working.

With this features as the specifications of the system, this is the main objective of this work:

- Propose a dual-mode, common-hardware, UWB-based platform for RPM systems in order to minimize its costs and power consumption.

- Verify it by means of simulation and experimental results to prove its viability.

1.3. System description and Methodology

A RPM system consists in a network composed by lots of nodes. Each node has two modes of operation: the data transmission one (DTM) and the radar one (RM). The first one allows the nodes to transmit and receive data (A in Fig. 1.2). The second one is in charge of measuring the phenomenon in question (B in Fig. 1.2). The structure of the nodes (red dotes in Fig 1.2) is depicted in Fig. 1.3.

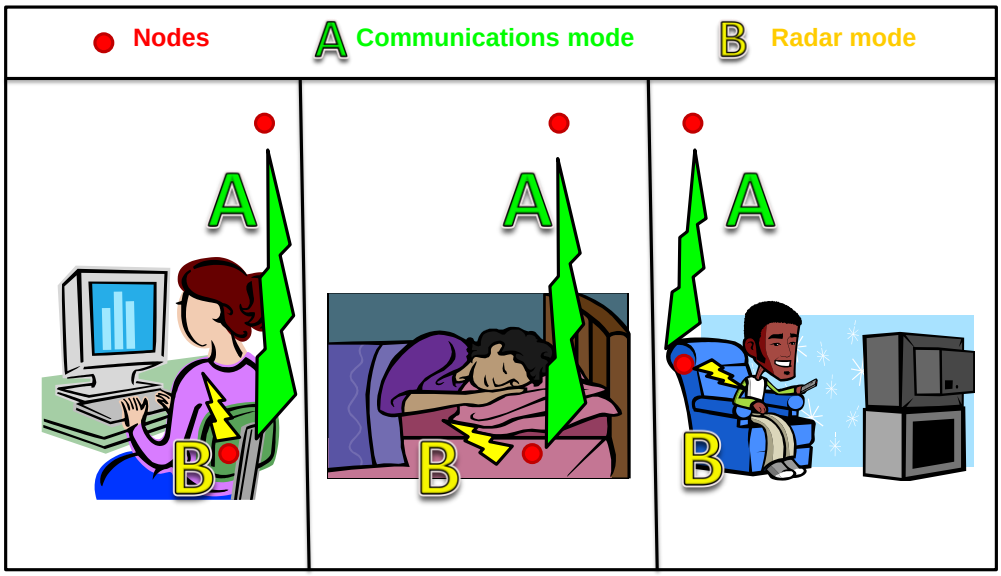

Fig.1. 2. Two modes of operation: communications and radar

Both modes consist of a transmitter, a channel and a receiver but these blocks are clearly differenciated for each mode. The transmitter of the data transmission mode emits a sequence of modulated pulses, while the one of the radar mode emits a train of pulses with no modulation at all. The channel for the data transmission mode must characterize the free-space propagation of the signal with its multipath replicas, whereas the one for the radar mode must take into account the different dielectric properties of the human tissues. The receiver of the data transmission mode has to demodulate the signal for

recovering the data, whist the one of the radar mode has to recover the signal for extracting the information of the monitored phenomena.

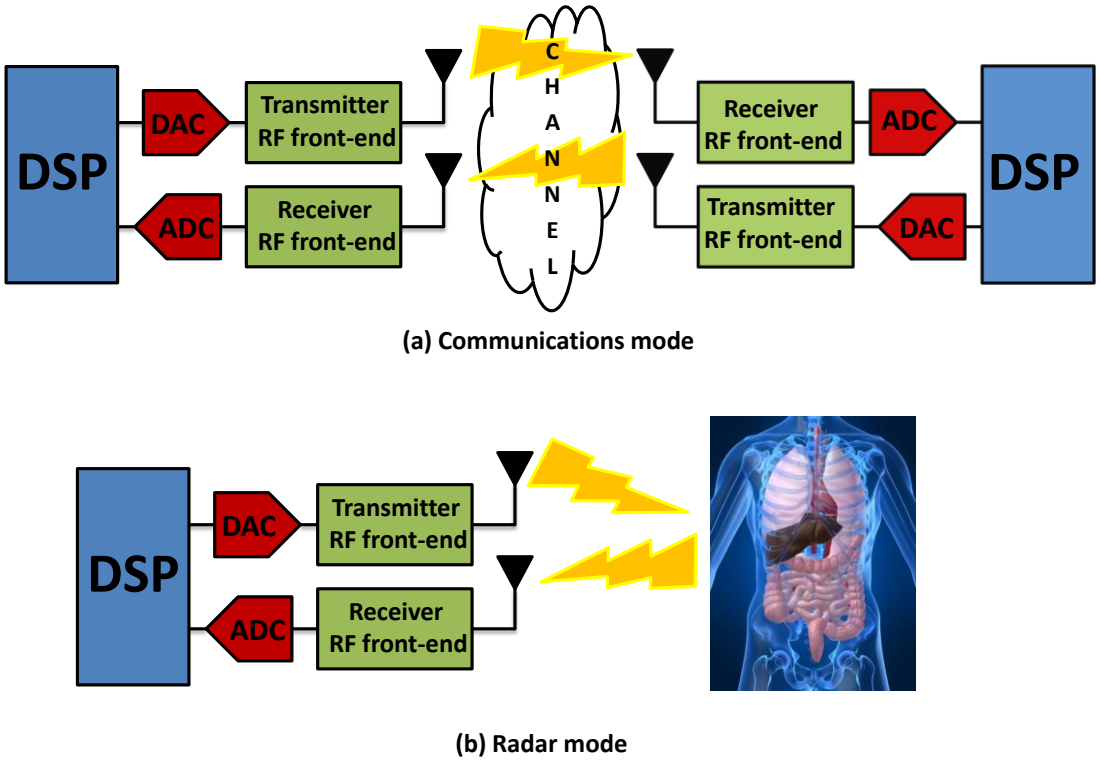

Fig.1. 3. Block diagram of the data transmission mode (a) and radar mode (b)

The communication between nodes has two functions: the transmission of the data obtained in the radar mode and the transmission of support commands that allow the proper working of the network. On the other hand, the radar mode depends on the monitored phenomenon. The hardware is the same, but the methods used to measure, for example, the heart rate are not valid when trying to obtain the amount of urine in the bladder.

1.4. Development tools

1.4.1. Software

1.4.1.1. Matlab / Simlink

This project was done by using Simulink® [5]. Simulink® is an environment for multidomain simulation and Model-Based Design for dynamic and embedded systems. It provides a customizable set of block libraries that let the user to

design, simulate, implement and test a variety of time/frequency-varying systems.

Simulink® is integrated with MATLAB® that provides access to an extensive range of tools that allow the user to develop algorithms, analyze and visualize simulations.

For a part of this work, the libraries from Xilinx® were used. Using MATLAB, the simulations were verified in order to be sure that the system was working properly. Once everything is verified, the Xilinx® System Generator for DSP® generates automatically the VHDL code for the Fast Programmable Gate Array (FPGA).

1.4.1.2. System Generator for DSP

The physical implementation has been done using the System Generator for DSP® of Xilinx®. The System Generator (XSG) is the leading software tool on the market of the Digital Signal Processing systems design with a FPGA.

Along with Matlab® and Simulink® from the company Mathworks®, XSG allows the creation and verification our system designs, which can be implemented aferwards in a FPGA.

The main features of the System Generator for DSP, used in this work, are the following ones [6]:

- **DSP modelling**: Use the Xilinx Blockset to build and debug DSP systems in Simulink®.
- **Bit and cycle accurate floating and fixed-point implementation.**
- **Automatic code generation of VHDL or Verilog from Simulink®.**
- **Hardware co-simulation**: An option that allows you to validate working hardware and accelerate simulations in Simulink and MATLAB.
- **Hardware / software co-design of embedded systems**: It provides a shared memory abstraction of the HW/SW interface, automatically generating the DSP the bus interface logic, software drivers, and software documentation.

1.4.2. Hardware

1.4.2.1. XtremeDSP Development kit for Virtex-4

A FPGA is a semiconductor device that contains logic blocks. The interconnection and functionality of these blocks can be programmed. The programmable logic goes from functions that can be performed by logic door to complex systems on a chip [7].

The FPGA used in this project to execute the code compiled by the XSG is a *Virtex* 4 of Xilinx® (Fig 1.4).

This has two independent 14-bit ADC channels capable of sampling rates up to 105 MSPS, and two independent 14-bit DAC channels capable of sampling rates up to 160 MSPS. This kit also has an input for an external clock. The kit is supplied with the Nallatech BenONE DIME-II motherboard, which supports USB interface performance. The XtremeDSP Pro kit is also supplied with the Nallatech FUSE system software that allows the management and control of the hardware.

Fig.1. 4. XtremeDSP Development kit for Virtex-4 [8]

1.4.2.2. Geozondas Radar Kit

As it is explained in chapter 4.3, the analog bandwidth of the ADC used for the XtremeDSP Development Kit is not enough to sample the Ultra-Wideband signals (high bandwidth, in the order of GHz). Therefore, an alternative way to get experimental results of the receiver is needed. The Evaluation Kit GZ6EVK consists of a useful set of instruments that could be use in a lot of applications, such as live object detection (RM) or data transmission (DTM).

The kit comes with a sampling converter, a pulse generator and a set of antennas that can work in the frequency range of 3.1-10.6 GHz. An image of the whole system can be seen in the Fig. 1.5.

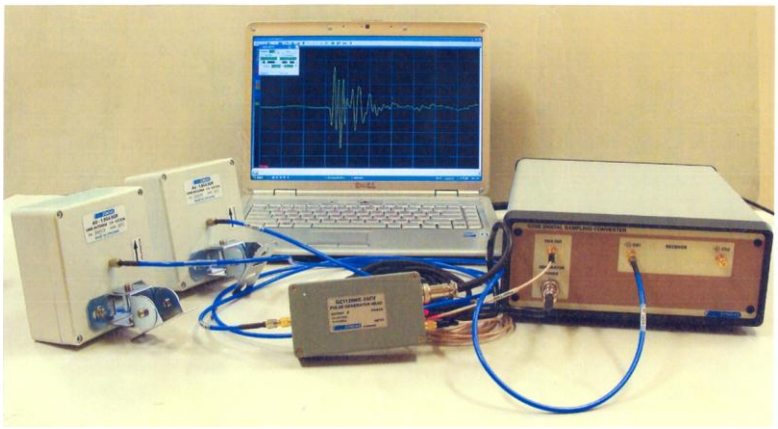

Fig.1. 5. Geozondas radar kit [9]

1.4.2.3. Transmitter RF front-end Pulse Generator

The transmitter of this work includes a pulse generator (PG). The pulse generator used is based on inserting frequency notches into the UWB power spectrum and is fabricated in a standard 0.18 µm CMOS process. The operation of the pulse generator is widely explained in [10]. Fig.1.6 shows the block diagram of the pulse generator, composed by two basic pulse generators and a time delay. In Fig.1.7 an image of the pulse generator is depicted. As it can be seen, it needs some external signals to work. Our labor is to supply the PG with the proper signals to achieve the desired signal at the output; with the correct frequency and power.

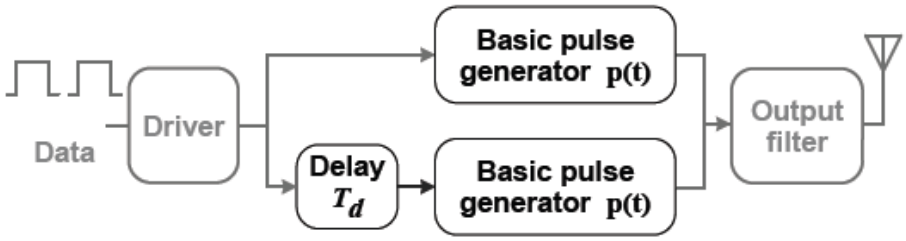

Fig.1. 6. Block diagram of the pulse generator [10]

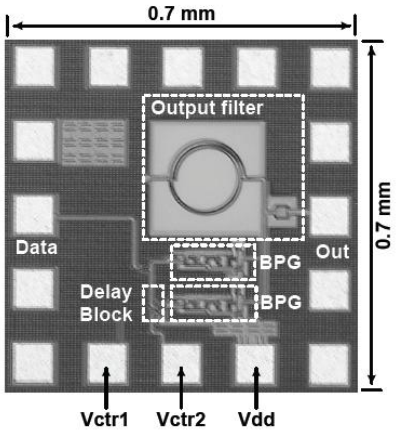

Fig.1. 7. Real image of the pulse generator[10]

CHAPTER 2. REMOTE PATIENT MONITORING SYSTEMS

Healthcare has evolved throughout the last two centuries. Here is a rough timeline to contextualize RPM systems. It has been extracted from Mike Barrett's presentation in the Sixth Annual Healthcare Unbound Conference & Exhibition held in Seattle (2009, www.tcbi.org).

- 18th Century and earlier: before the institutionalization of healthcare, doctors and caregivers would visit patients at home or at their work place.
- 19th Century: Pioneering hospitals like Massachusetts General Hospital developed big places of care that lead to the professionalization of healthcare.
- 1980s: Chronic care centers were introduced to improve the attention to people suffering from those diseases.
- 1996: Kaiser Permanente (www.kaiserpermanente.org) launches an online health site to instruct its members on how to access care.
- 1999: RPM began with devices connected to the telephony lines.
- 2002: Forrester Research authors a report in which a trend to de-institutionalize the healthcare is detected. A return to its roots.

2.1. Introduction to RPM

RPM, telemedicine and eHealth are hyponyms of telehealth. While telemedicine typically envolves a real-time contact with a physician and it is aimed at the curative aspect, RPM is mainly focused on the preventive aspect and does not imply a direct contact between the patient and the health professional. As for eHealth, it is just a concept referring to Internet-based teleheath services [11].

Once the concepts are clearified, the Venn diagram in Fig. 2.1 shows the three main components of a telehealth system.

Firstly, the people group includes patients, health professionals, administrators, researchers, etc. Secondly, telecommunications & network links are responsible for connecting the main and the remote locations. That connection can be done, for instance, through telephony, the Internet and Virtual Private Networks (VPN), High speed digital networks or point-to-point dedicated facilities. And finally, telehealth application technology is the collection of hardware, software and peripheral devices that enable the working of the system. The main work of this thesis is enshrined in this last group, particularly, as it was stated in Chapter 1, in the monitoring equipment in charge of obtaing and forwarding data from the patient.

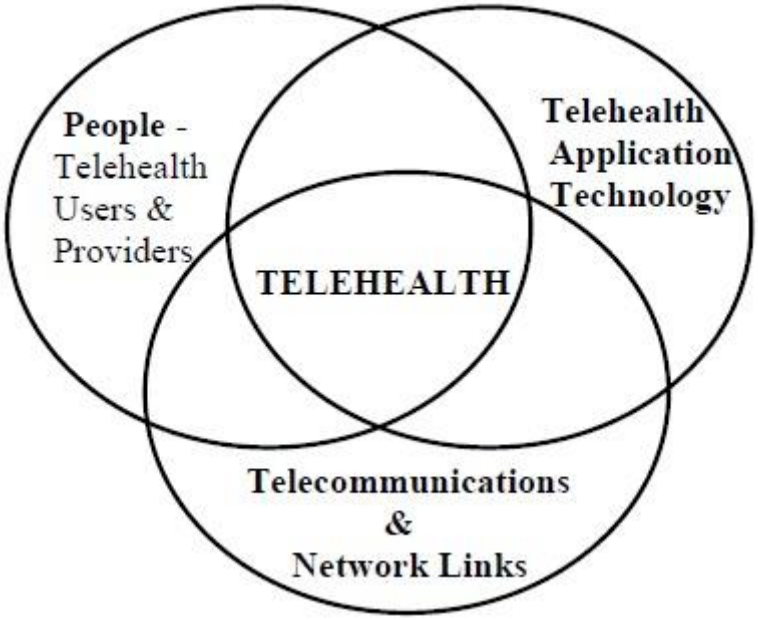

Fig.2. 1. Components of a telehealth system[11]

2.1. State of the art

As it is such a wide and hot topic, there are constant research innovations that a survey of the state of the art is not an easy task. This section is aimed at illustrating some of the main existing methods used in this kind of equipment. Two main functions can be distinguished: sensing and communications.

2.1.1. Sensing

For the sensing function, the collaboration of the patient is always required to a greater or lesser extent. Monitoring diseases such as depression requires the patient's interaction with a computer with, for instance, an Interactive Voice Response (IVR) system. However, other chronic diseases can be monitored in a way the patient scarcely notices. This depend a lot on the monitored disease thus in the measured parameter. Furhermore, some of those parameters can have a contactless measurement and some of them do not. Contactless measurements are more comfortable for the patient but, in some cases, their accuracy is lower than in their respective contact readings.

Among all the phenomena, five parameters have been chosen in this section: temperature, heart rate, respiration rate, glucose in blood and water accumulation in the body. Here is a brief exposition of these parameters and some of the methods used for carrying their monitoring out.

2.1.1.1. Temperature

An abnormal body temperature may be due to external or internal factors. On the one hand, a long exposure to high or low temperatures leads to hyperthermia or hypothermia, respectively. Both situations can cause severe damages to the patient. On the other hand, it can reveal the reaction of the body to a certain infection, virus or other illnesses.

The most known a spread method is the traditional mercury thermometer. It is introduced in the mouth, under the arm or in the anus thus requires the contact with the body. A newer solution is based in infrared. For high accuracy, an infrared ear thermometer measures the radiated energy by the subject's eardrum, which is situated close to the hypothalamus, the core temperature regulator of the body. Despite the high accuracy provided, it needs to be introduced in the ear of the patient. Another method to avoid this is the infrared thermal imaging. Although it does not provide a high accuracy since can be affected by other radiation sources, it is a contactless measurement whose benefits have already been stated [12].

2.1.1.2. Heart rate

The monitoring of the heart rate can reveal a heart failure or alert the patients to an abnormal heart behavior that can threaten their lives.

The traditional method is to measure the number of beats in an artery close to the skin, usually the radial or the carotid (in the wrist and the neck respectively). This method requires on-body equipment [12]. The alternative is radar monitoring in which UWB radar is especially suitable [13].

Nevertheless, in certain cases, measuring the rate is not enough. When there is the need to monitor the heart beat pattern and its strength, Electrocardiographies (ECG) or electroencephalographies (EEG) are required. This typically implies the use of electrodes in contact to the body of the patient but the use of capacitive electrodes allows non-contacting ECGs such as the "Aachen SmartChair" [14].

2.1.1.3. Respiration rate

Measuring the respiration rate can be used for monitoring chronic lung diseases such as asthma and can help detecting others like pneumonia or congestive heart failure [12].

The easiest method to monitor the respiration rate is by counting the number of expansions and contractions of the thorax. As for the heart rate, UWB radar is also a possible solution.

2.1.1.4. Glucose in blood

For people suffering from diabetes or hypoglycemia, blood glucose monitoring (HBGM) is vital.

The currently used glucometers are uncomfortable for the patients. They require a blood sample to measure the amount of glucose. Nowadays, alternative, non-invasive methods are being developed. Infrared, ultrasonic and electromagnetic technologies are used to make it possible. An example is the device GlucoTrack™ by Integrity Applications, which is still in clinical trials phase [15].

2.1.1.5. Water accumulation in the body

The possibility of detecting water presence in the human body is useful for diagnosing diseases such as pulmonary edema, ascites or liver cirrhosis and for monitoring other pathologies like urinary retention or incontinence by measuring the urine accumulation in the bladder [16].

One more time, UWB radar is a potential solution. Unlike urinary catheterization, UWB radar is non-invasive thus urinary tract infections are avoided.

The water accumulation in the human body will be the phenomenon monitored by the radar mode presented in this thesis.

2.1.2. Communications

Once the data is obtained, the need for its transmission arises. There are several technologies and protocols available. Each of them is optimized for a certain situation but can also be adapted to new scenarios. The most known are [12]:

- Bluetooth
- WiFi (IEEE 802.11)
- ZigBee
- UWB
- WiMAX (IEEE 802.16)
- Radio Frequency Identification (RFID)
- Infrared (IR)
- Cellular networks (GSM, CDMA, EVDO, EDGE, …)

The first four will be compared in section 3.1 in order to justify the selection of UWB in this thesis.

2.2. Limitations

RPM systems are still not widely adopted. They can potentially be applied to homes, hospital and mobile devices; however, it has not been done yet. Here are some of the possible causes:

- **Cost**: the present solutions are still expensive. Government policies are needed for RPM systems to become part of people's life.

- **Reticence**: Some of the people involved in telehealth (first group in section 2.1), such as some patients and health professionals, do not trust in RPM systems. Their fully involvement is required for these systems to succed.

- **Standarization**: The lack of a generally accepted standard translates into incompatibilities between solutions by different manufacturers.

- **Telecommunications infrastructure**: Mainly in rural areas, the links enabling the transmission of the data collected from the patient is unviable because the infrastructure is missing.

2.3. Clinical trials

Despite not being widely adopted, clinical trials have been done to prove the efficiency of RPM systems. One of the largest was carried out by the United Kingdom's Department of Health. It was named the Whole System Demonstrator [17]. The early headline findings of December 2011 show that if telehealth is used correctly, it can deliver:

- 15% reduction in Accident & Emergency visits.
- 20% reduction in Emergency admissions.
- 14% reduction in elective admissions.
- 14% reduction in bed days.
- 8% reduction in tariff costs.
- 45% reduction in mortality rates.

CHAPTER 3. ULTRA-WIDEBAND

3.1. Why Ultra-Wideband (UWB)?

In this section, a discussion about the selection of UWB technology will be done through a comparison between wireless technologies in both for the two operation modes. These are technologies that will be compared:

- UWB
- Zigbee
- WiFi
- Bluetooth

First of all, in the Fig. 3.1, a comparison between the nominal ranges of these four technologies is done:

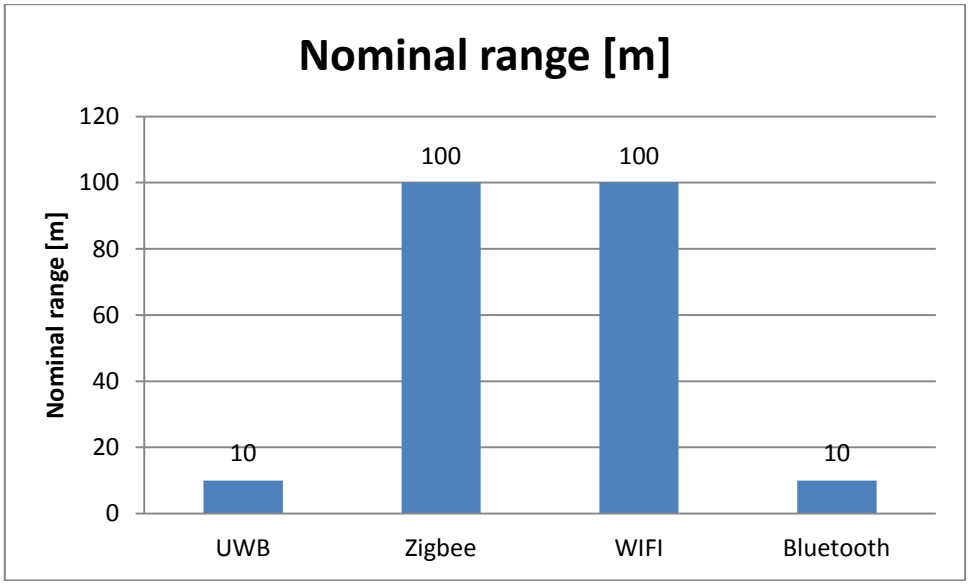

Fig.3. 1. Wireless techonologies nominal range

[Source: A comparative study of wireless protocols: Bluetooth, UWB, Zigbee and WiFi by ITRI]

Secondly, in Fig. 3.2 and 3.3, a comparison between the power consumption of the different technologies is shown. Fig. 3.2 shows the power consumption in mW and Fig. 3.3 shows the power consumption in terms of nJ/bit.

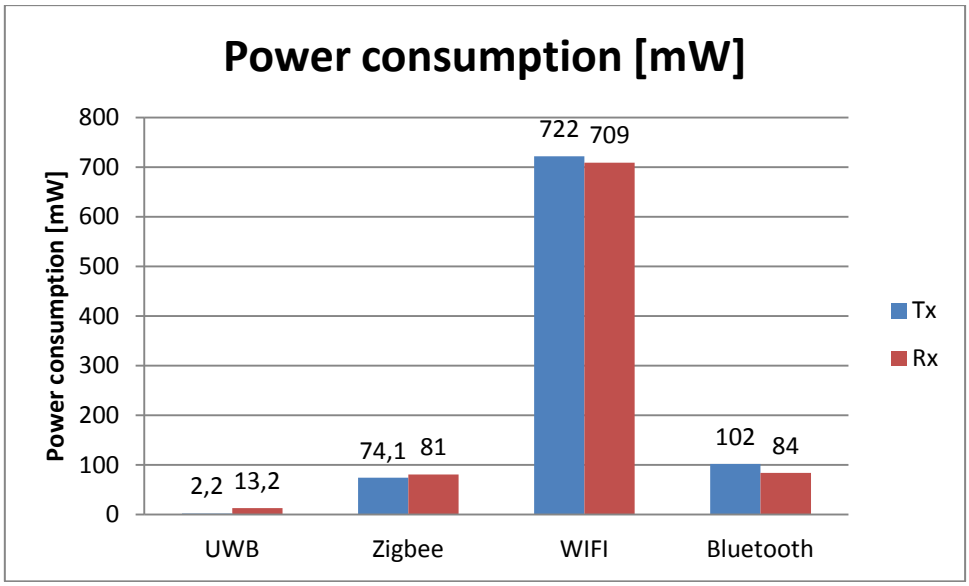

Fig.3. 2. Wireless techonologies power consumption in mW

[Source: Low Power UWB System and Circuits Designs for WSNs by Ming Shen]

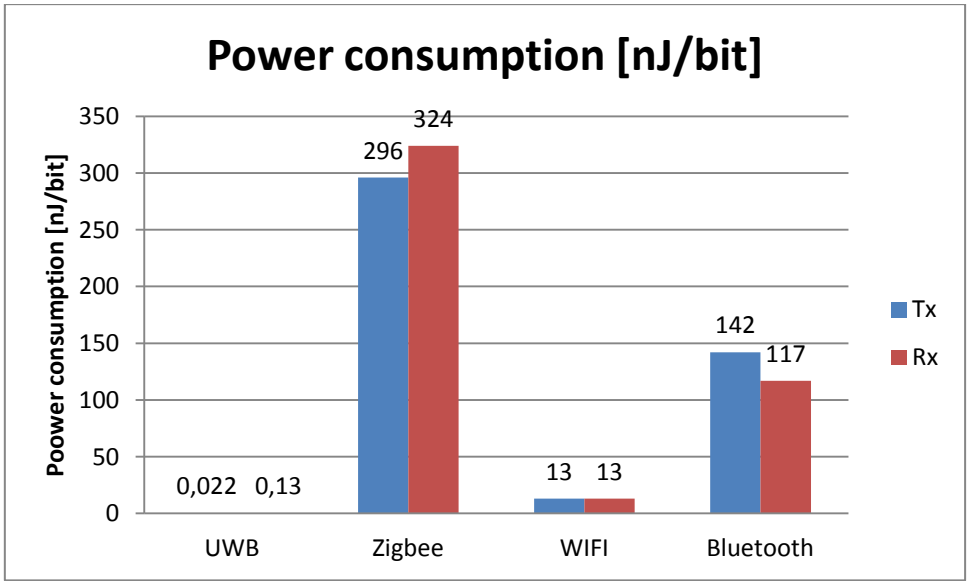

Fig.3. 3.Wireless technologies power consumption in nJ/bit

[Source: Low Power UWB System and Circuits Designs for Wireless WSNs by Ming Shen]

Thirdly, in the Fig.3.4, the sample rates are compared:

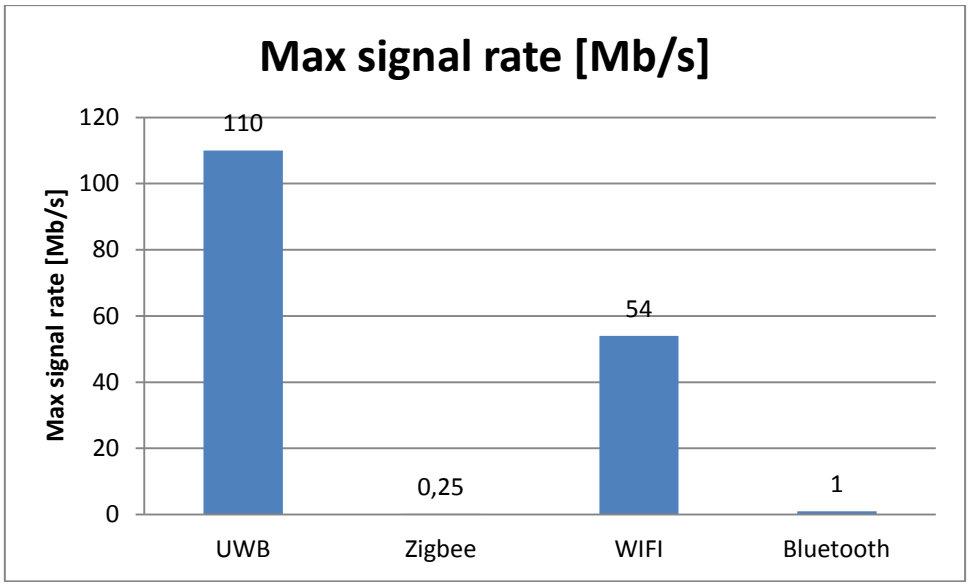

Fig.3. 4.Wireless technologies max signal rate

[Source: A comparative study of wireless protocols: Bluetooth, UWB, Zigbee and WiFi by ITRI]

And finally, in the Fig.3.6, the channel bandwidth comparison can be seen.

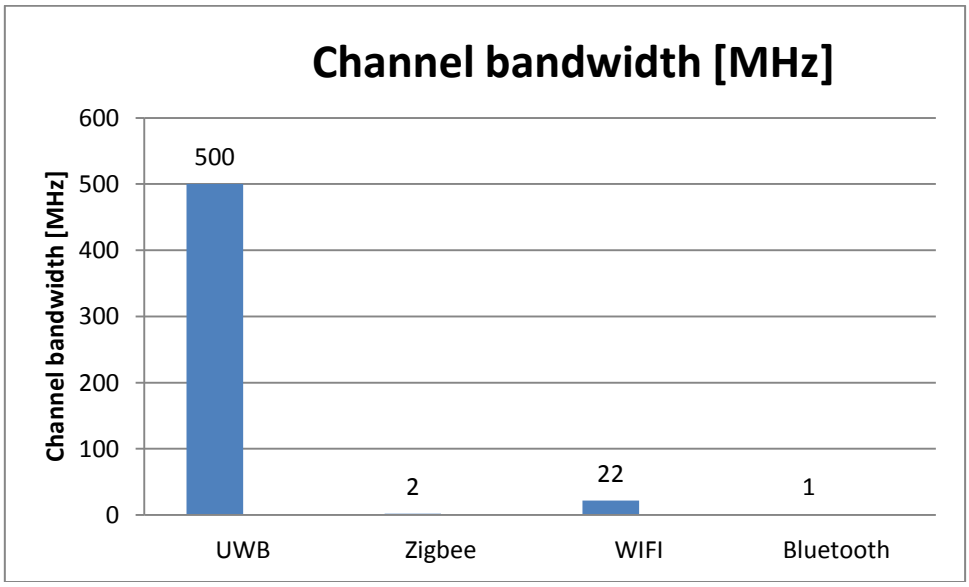

Fig.3. 5. Wireless technologies Channel Bandwitdth

[Source: A comparative study of wireless protocols: Bluetooth, UWB, Zigbee and WiFi by ITRI]

Watching these figures, it is concluded that UWB is the wireless technology that best fits our project requirements. As can seen in the figures above, this technology has the lowest power consumption, has the highest signal bit rate and the largest channel bandwidth. The only problem could be that its nominal range is not very high, but for RPM applications, 10 m of range could be enough.

If we get focused in the RM of our system, the higher resolution of the UWB radars is the main reason to choose UWB against other wireless technologies [18].

The increased resolution in this kind of radars is because UWB pulses have durations of nanoseconds (ns), while other wireless technologies pulses have durations of microseconds (μs).

Some advantages of the UWB radar are listed below [18]:

- Improve radar resolution.
- Reduce the radar passive interferences, such as, rain and mist. This is because the scattering cross section of interference source within a small pulse is reduced.
- Improve the radar's immunity against other wireless signals effects and noise.
- Decrease the radar "dead zone"

3.2. History

In order to contextualize the selected technology, a brief history is presented in this section.

UWB seems to be a new technology, but his origin comes from the early days of radio [19].

- 1987: Marconi invents the first UWB system, the Spark-Gap transmitter.
- 1973: Fundamental patent of UWB (Ross).
- 1974: UWB radar for subsoil penetration is designed by Morey.
- 1989: The concept of UWB as is known today is introduced by the Department of Defense of the US.
- 1990: Withington design UWB point-to-point radios.
- 1992: Multiple access UWB radios are designed by Scholtz in University of South California (USC).
- 1996: First UWB laboratory in a university (USC).
- 2002: FFC authorize the use of UWB.
- 2006: IEEE 802.15.3a publications of MultiBand OFM UWB (MB-OFDM) and Direct-Sequence UWB (DS-UWB).
- 2008: Intel gives up with UWB development.
- 2010: Some companies interested in UWB: Samsung, NET, CSR, Realtek.
- 2013: UWB is expected to be used in industrial and medical nodes

Interest in UWB technology revived since the Federal Communications Comission (FCC) published their First Report and Order on February 14, 2002, in which the spectrum for UWB devices was allocated. The report authorized

the use of UWB in the frequency range from 3.1 to 10.6 GHz and power spectral density emission limit on -41.3 dBm/MHz. However, the emission limit for UWB emitters may be significantly lower (as low as -75.3 dBm/MHz) in other segments of the spectrum. All this restrictions could be seen in the FCC mask. (Fig.3.6).

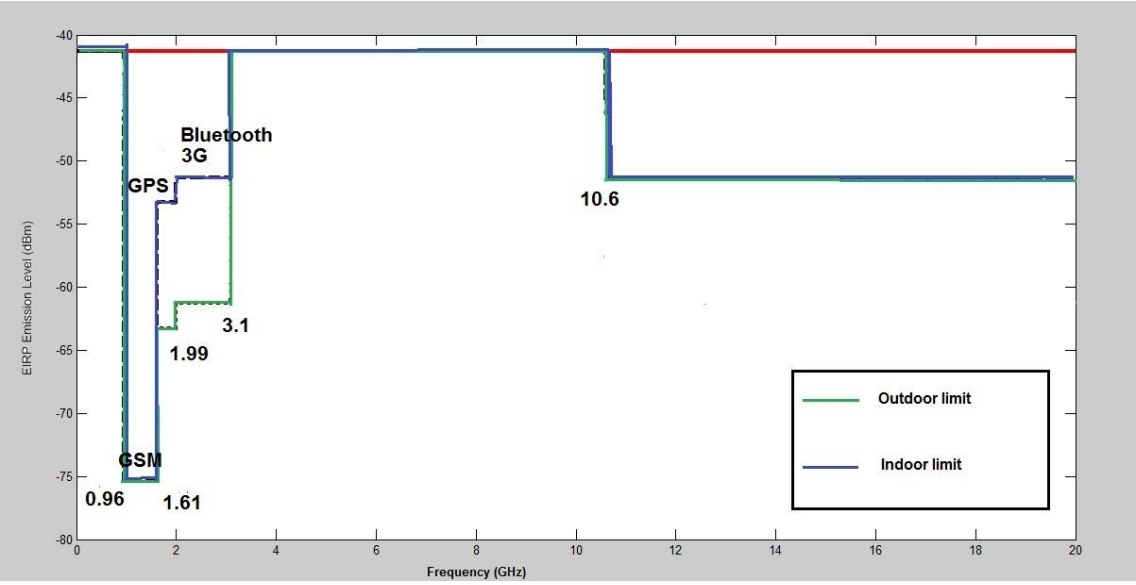

Fig.3. 6. FCC mask for UWB applications.

3.3. Description

This technology is a wireless technology that transmits large amounts of digital data over a very wide spectrum of frequency (BW ≥ 500MHz) with low power consumption in a low distance range.

UWB is based on transmitting very short-duration pulses, typically with a duration of nanoseconds, which translates into a very high occupied bandwidth (Fig.3.7). This allows achieving data rates of hundreds of Mbps, while using the same bands as other existing communication technologies, without producing significant interference.

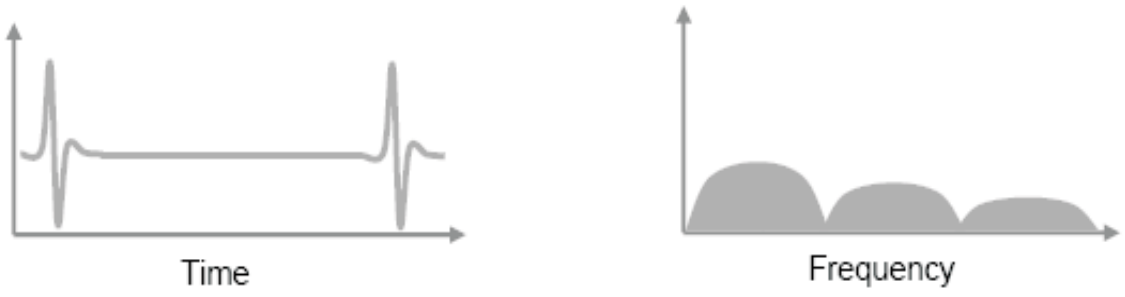

Fig.3. 7. Ultra-wideband signals in time and frequency domain [20]

3.4. Applications

Ultra-wideband can be use in multitude of applications [20]. We can divide these applications in data transmission applications and radar applications.

UWB data transmission applications are part of the Wireless Communications Systems. The main characteristic of this systems using UWB is that the network has scalable speeds, from low to ultra-high. Moreover, it has a cheap architecture and low power consumption. Some Wireless Communications Systems that could be built using UWB are the following ones:

- High speed local and personal area networks (WLAN/WPAN)
- Roadside info-station
- Short range radios
- Military communications

In radar applications, UWB has been used for a long time. Many measurement tools work with this technology, such as, fluid level detection, collision warning avoidance and wall thickness measurement.

As we said before, the operation of these applications consists in transmitting very short pulses very rapidly. This operation is really attractive because the radar resolution increases thus can detect small size objects. Consequently, several small targets that are located together can be identified separately with UWB, while other technologies, with lower resolutions, could identify them as a single object.

UWB radars are being developed for new types of imaging systems that would be used by rescue personnel to locate persons hidden behind walls, under debris or avalanches. These radars are also being used in medical monitoring as it was explained in the previous chapter.

Some radar applications are listed below:

- Vehicular & collision avoidance radars
- Ground penetrating radar (GPR)
- Through wall imaging (Police, Fire, Rescue)
- Medical imaging and monitoring
- Surveillance

3.5. IR-UWB

Two types of UWB are Multi-Band-OFDM UWB and Impulse-Radio UWB (IR-UWB). For this work, IR-UWB has been selected after studying both forms.

MB-OFDM is a multi-band technology using orthogonal frequency division multiplexing [21]. The main difference between both forms of UWB is that MB-OFDM transmits data at the same time over multiple carriers, while IR-UWB transmits without the need of carrier. Some benefits of MB-OFM are high spectral flexibility and resistance against RF interferences and multi-path

effects. On the other hand, the main drawback is that the need of a carrier limits the applications in some practical cases, since the frequencies that could be used are limited.

The advantages supporting the selection of IR-UWB are the following ones [22]:

- Transmission of ultra-short duration pulses, on the order of ns.
- Power efficiency due to its low duty cycle, i.e. low power consumption.
- Carrierless transmission.
- Scalable data rates versus distance.
- Ease of implementation of the transmitter and the receiver.
- Robust against multipath propagation.

There are many modulations that could be use to transmit IR-UWB pulses. For this work was chosen ON-OFF Keying (OOK).

OOK is included in amplitude-shift keying modulations. This modulation is represented by the transmission or no transmission of the pulse (Fig.3.8). The main advantage of this modulation is that the power consumption is lower, 50% in average, than for other modulations. In this work, a particular case of OOK named Synchronized-OOK (S-OOK) is also used. In this case, synchronization pulses are added to the OOK data pulses and both are transmitted. The synchronization pulses are always present, while the data pulses only when the bit is a ‘1’ (Fig. 3.9).

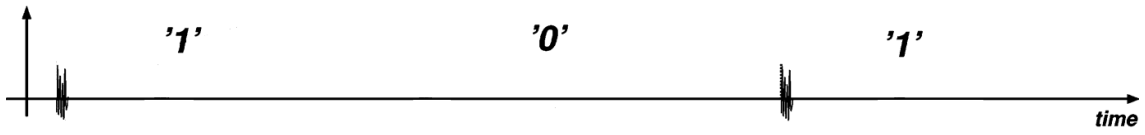

Fig.3. 8. OOK modulation [23]

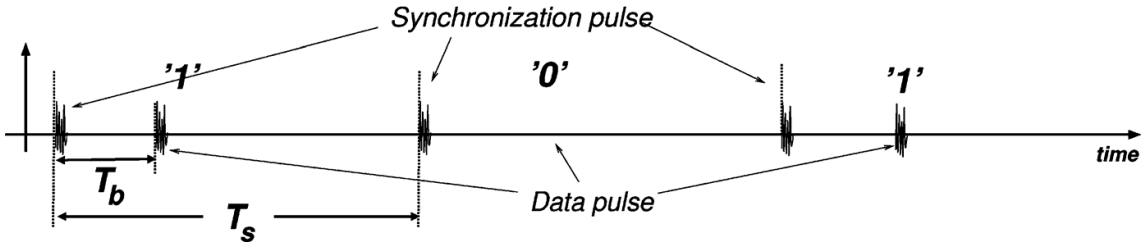

Fig.3. 9. S-OOK modulation [23]

CHAPTER 4. SYSTEM DESCRIPTION, IMPLEMENTATION AND RESULTS

4.1. Transmitter

The transmitter, whose block diagram can be seen in Fig. 4.1, uses the same hardware for both operation modes. This is possible because the radar mode is a particular case of the data transmission mode, in which the signal is periodic. That means sending only bit '1' if using OOK modulation, or bit '0' for S-OOK modulation.

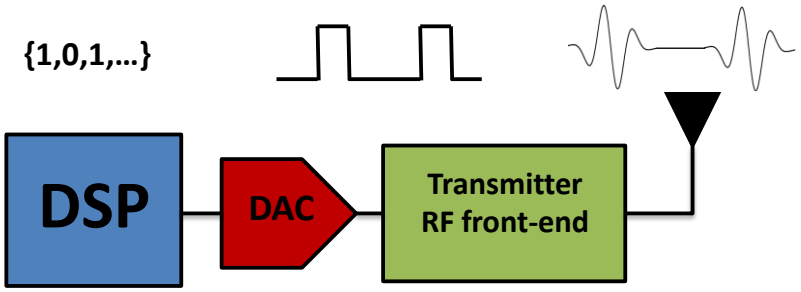

Fig.4. 1. Block diagram of the transmitter

Apart from keeping the energy consumption as low as possible, the main restriction for the transmitter is to fulfill the FCC mask. Its shape was introduced in section 3.2 but table 4.1 describes its boundaries accurately.

Table 4.1. FCC radiation limits for indoor applications [24].

Frequency in GHz	EIRP in dBm/MHz	EIRP in dBm/Hz
Below 0.96	– 41.3	– 101.3
0.96 – 1.61	– 75.3	– 135.3
1.61 – 1.99	– 53.3	– 113.3
1.99 – 3.1	– 51.3	– 111.3
3.1 – 10.6	– 41.3	– 101.3
Above 10.6	– 51.3	– 111.3

In order to meet the FCC requirements, three characteristics must be properly adjusted since they modify the spectrum of the signal: the pulse waveform, its amplitude and the bit rate. The first one changes the shape of the spectrum, while the other two prompt a shifting in the Y-axis.

In the literature, one can find several different waveforms for UWB systems. In [25], some of the most used waveforms are described and compared. They are: the gaussian pulse, the gaussian monocycle, the Scholtz's monocycle, the Manchester monocycle, the RZ-Manchester monocycle, the sine monocycle and the rectangular monocycle. Nevertheless, those are not the only ones. For our system, the 5^{th} derivative of the gaussian pulse has been chosen. The waveforms and the power spectral densities (PSD) of the Gaussian pulse and

its 5th derivative are depicted, in blue and red respectively, in Fig. 4.2. It is important to notice how the 3 dB bandwidth has moved from 0-2 GHz to 3.5-6.5 GHz. It is the first step to fulfill the FCC mask.

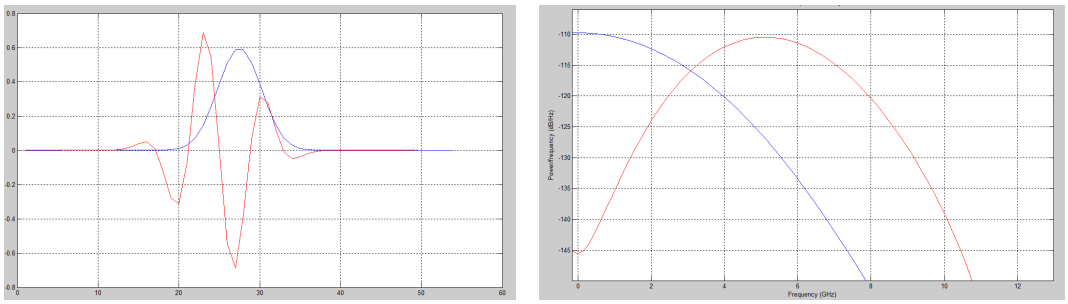

Fig.4. 2. Gaussian pulse (blue) and its 5th derivative (red) waveforms and PSDs generated with MATLAB®.

The second step is setting the amplitude and the bit rate. These two parameters determine the power of the signal. This average power of the signal can be calculated, applying the formula 4.1, as the bit energy times the bit rate:

$$P_{avg}[\mathrm{W}] = E_b[\mathrm{J}] \cdot R_b[\mathrm{bps}] \quad \textbf{(4.1)}$$

The bit energy is defined, in the equation 4.2, as the average number of pulses per bit times the pulse energy. For OOK, there is a pulse for bit '1' and no pulse for bit '0' thus the average number of pulses per bit is 0.5:

$$E_b[\mathrm{J}] = average\ pulses/bit \cdot E_p[\mathrm{J}] \quad \textbf{(4.2)}$$

The average number of pulses per bit is obtained with the formula 4.3 as a function of the bit '0/1' probability. For the data transmission mode, assuming the same probability for both bits (0.5), for OOK, there is one pulse for bit '1' and no pulse for bit '0' thus the average number of pulses per bit is 0.5. However, for S-OOK, two pulses represent bit '1' and one represents bit '0'. Therefore, in this case, there are 1.5 pulses per bit in average. For the radar mode, there is one pulse per bit:

$$average\ pulses/bit = p_{(0)} \cdot pulses/(0) + p_{(1)} \cdot pulses/(1) \quad \textbf{(4.3)}$$

Finally, equation 4.4 is used for calculating the pulse energy:

$$E_p[\mathrm{J}] = \int_0^{T_p} |x(t)|^2 \cdot dt \quad \textbf{(4.4)}$$

Once all the concepts are clearified, the implementation of the transmitter will be shown. It is divided in two stages, simulation and experimental, because the blocks used are different for each stage. The reason is that the Simulink blocks used for the simulation stage are not valid for the implementation in the Xtreme DSP Development kit. In this second case, the only blocks, which can be used, are the ones from the Xilinx Blockset.

4.1.1. Simulation Stage

As it was said before, the only difference in the transmitter, between the two operation modes, is that the transmitted message in the radar mode is all zeros or all ones depending on the modulation. Despite that fact, the same structure consisting of a different section for each mode is also used in this chapter.

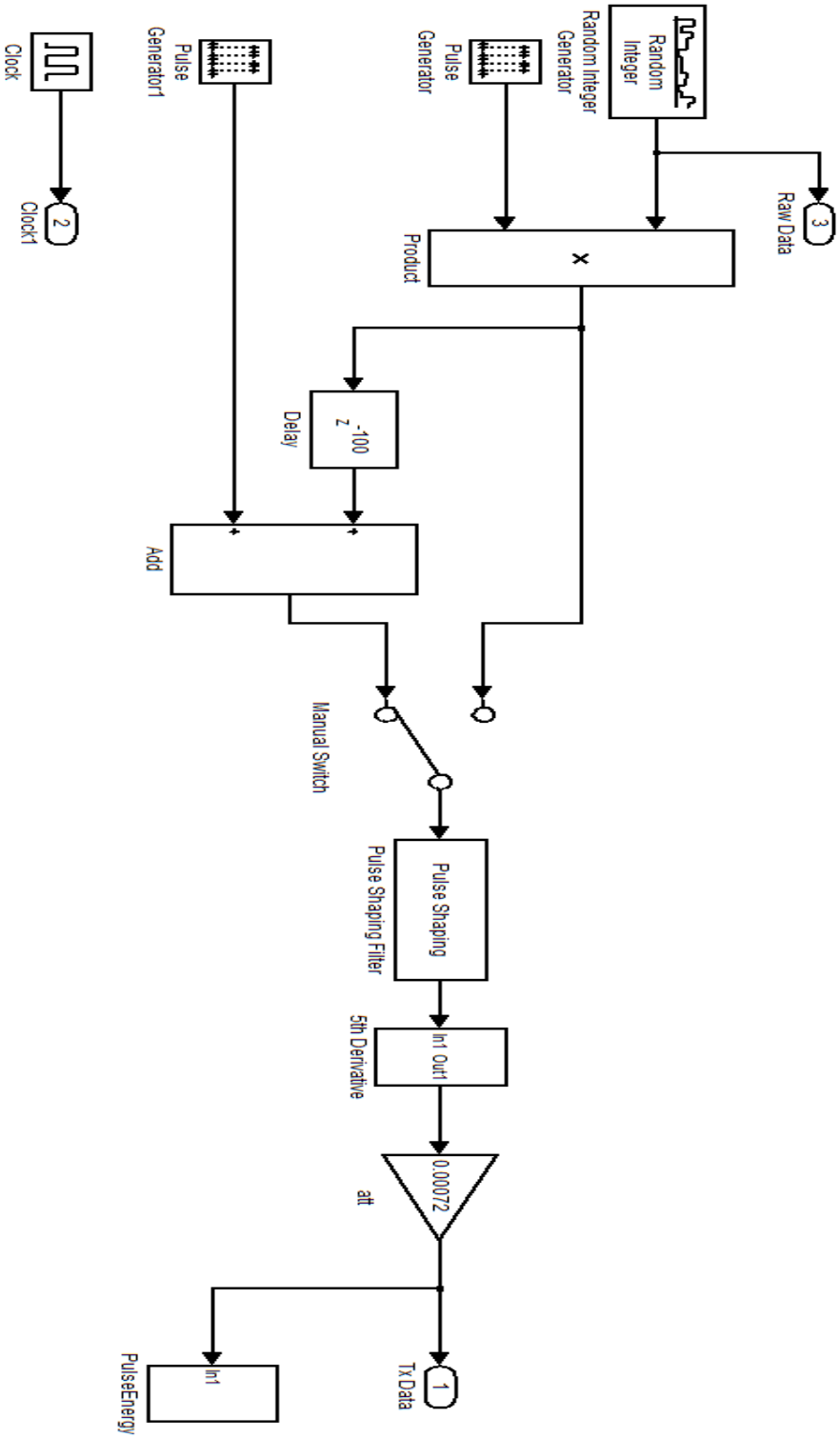

Fig.4. 3.Block diagram of the transmitter.

.

In Fig. 4.3, the block diagram of the transmitter is shown. The switch allows selecting the modulation between S-OOK (in the position of the picture) and OOK (if connecting the upper branch). The only difference between both modulations is that, for S-OOK, the data pulse is delayed and a synchronization pulse is added to the signal. After the switch, the Pulse Shaping Filter transforms the shape of the pulses from rectangular to gaussian. Then, the signal is derived to obtain the desired 5th derivative of the gaussian pulses (see Fig. 4). Finally, an attenuator is added for fixing the right amplitude at the output.

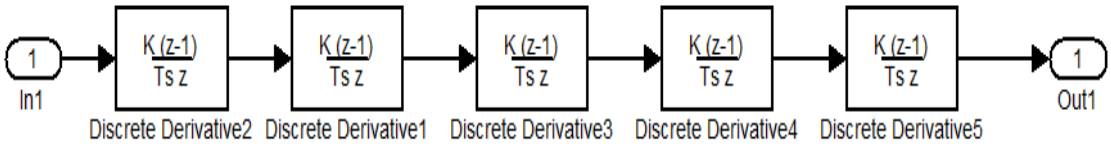

Fig.4. 4.Block diagram of 5th derivative subsystem.

4.1.1.1. Data transmission mode

Here are the simulation results for the data transmission mode. The Fig. 4.5 shows the three signals of the OOK branch corresponding to a {0, 1, 0} sequence. The first one is the output of the Random Integer Generator, which holds the value for the whole bit time. The second one is the pulse train, whose pulses have a width much smaller than the bit time. The product of these two signals properly aligned is the third signal that can be seen in the figure, which corresponds to the OOK modulated signal.

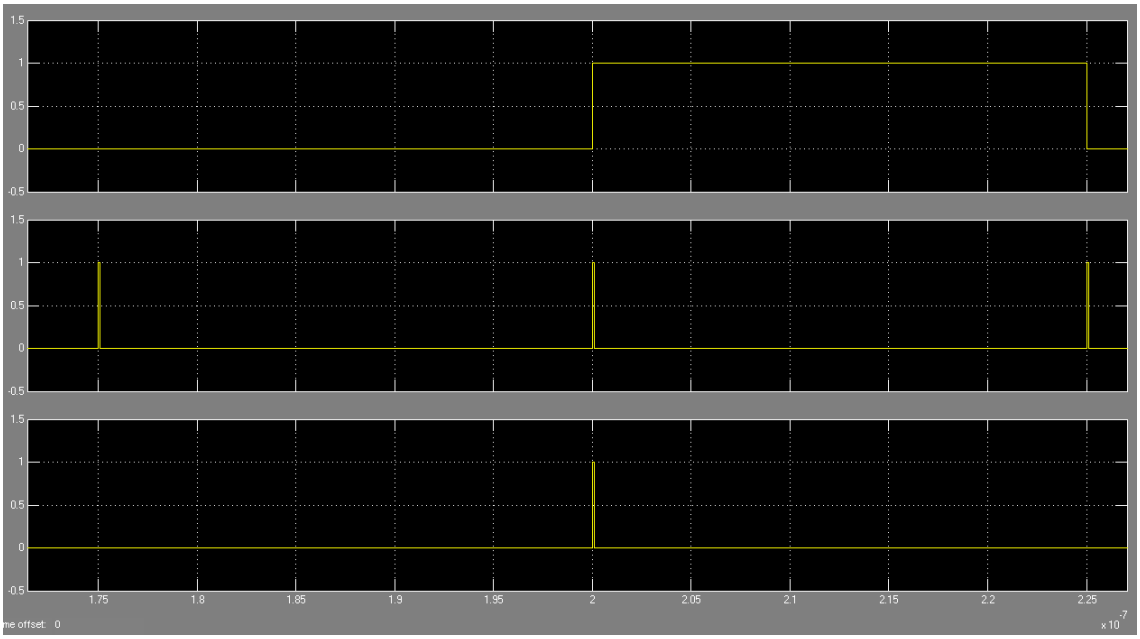

Fig.4. 5. OOK composing signals in the time domain.

In Fig. 4.6, the pulse shaping process is depicted. The rectangular pulse of the first plot is filtered and becomes the gaussian pulse of the second one. Then, it is derived five times and the resulting pulse can be seen in the third plot.

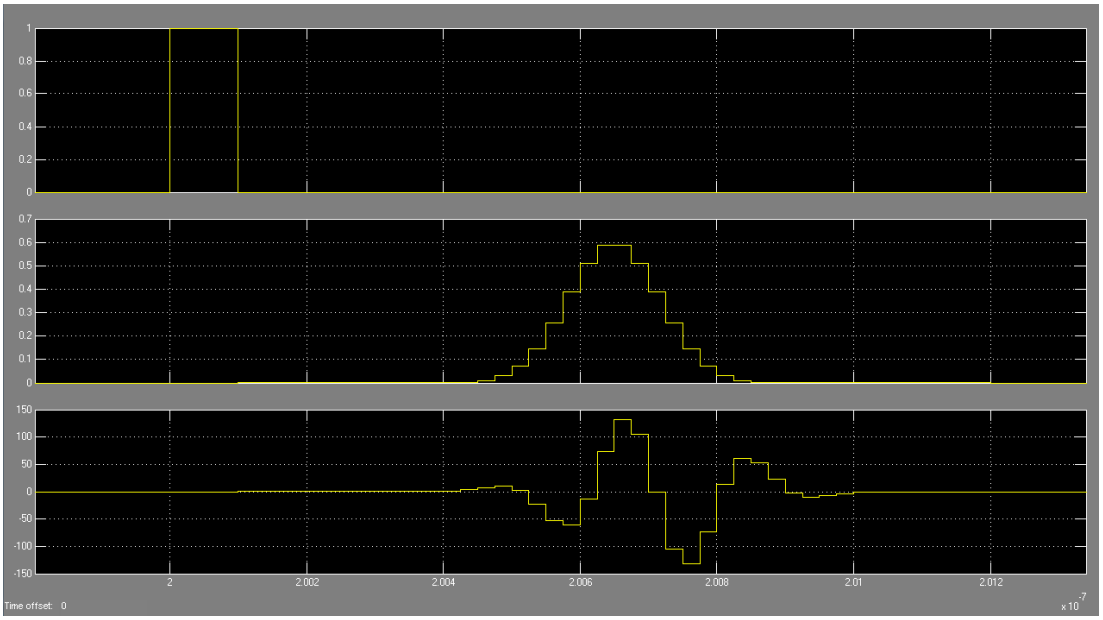

Fig.4. 6.Time domain signals through the shaping process.

Lastly, Fig. 4.7 shows the decomposition of the S-OOK signal. The first two plots show the synchronization and data pulses, whereas the last two show the addition of the two kinds of pulses and the amplitude correction.

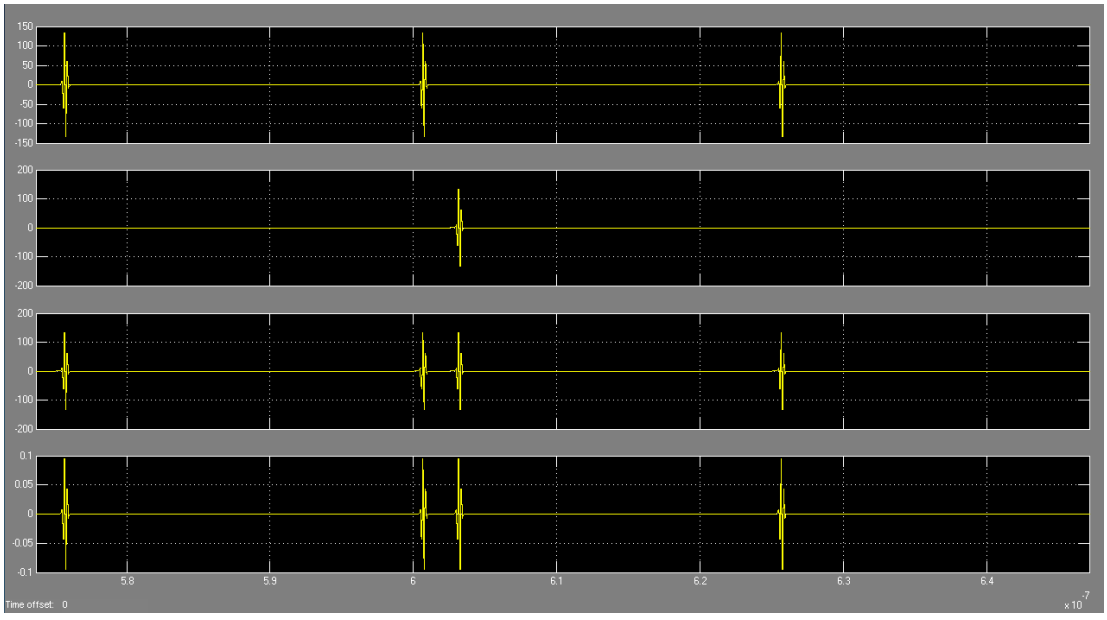

Fig.4. 7. Breakdown of the S-OOK signal.

To calculate the power of the transmitted signal, the “Pulse Energy” subsystem was made (at the right in Fig. 4.3). Its block diagram can be seen in Fig. 4.8. It is the implementation of the equations 4.1 to 4.4. Firstly, the signal is squared

and multiplied by the differential of time to be integrated. As it is a real-time windowed integration with a window equal to the pulse width, the maximum value at the output of the integrator will be the pulse energy. Multiplying it by the average number of pulses per bit and dividing it by the bit time, which is equivalent to multiply by the bit rate, one obtains the average power of the signal.

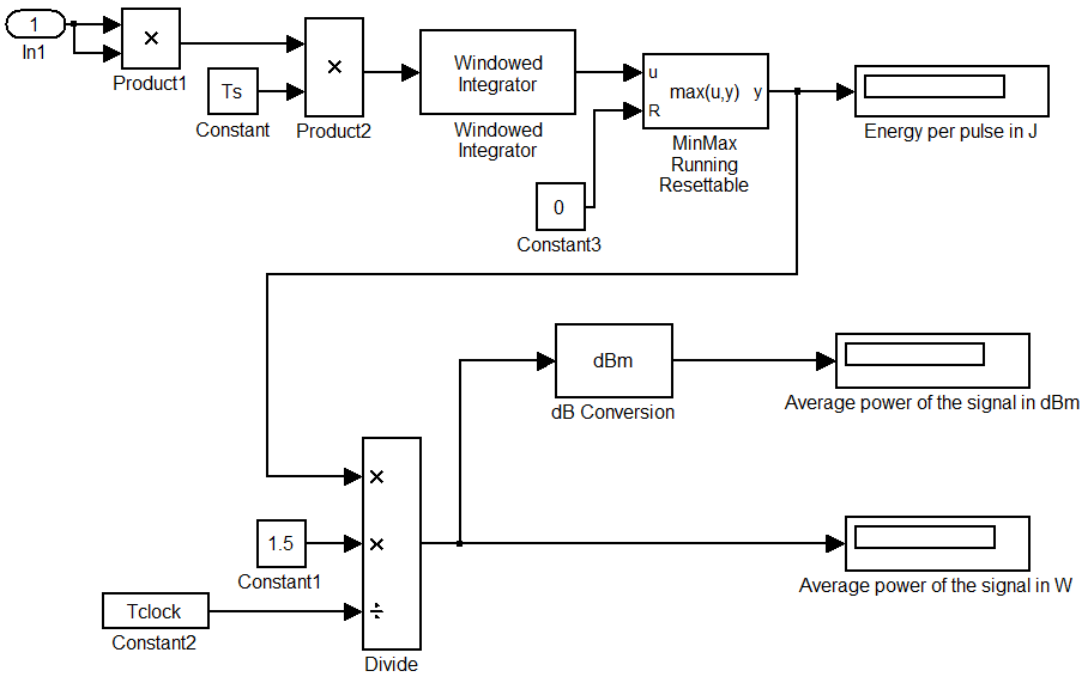

Fig.4. 8.Block diagram of the Pulse Energy subsystem.

Finally, the PSD of the S-OOK simulated signal is shown in Fig. 4.9. The red line depicts the FCC mask detailed in Table 4.1. Therefore, with a bit rate of 40 MHz and an amplitude of 0.1 V, the simulated signal fulfills the requirements.

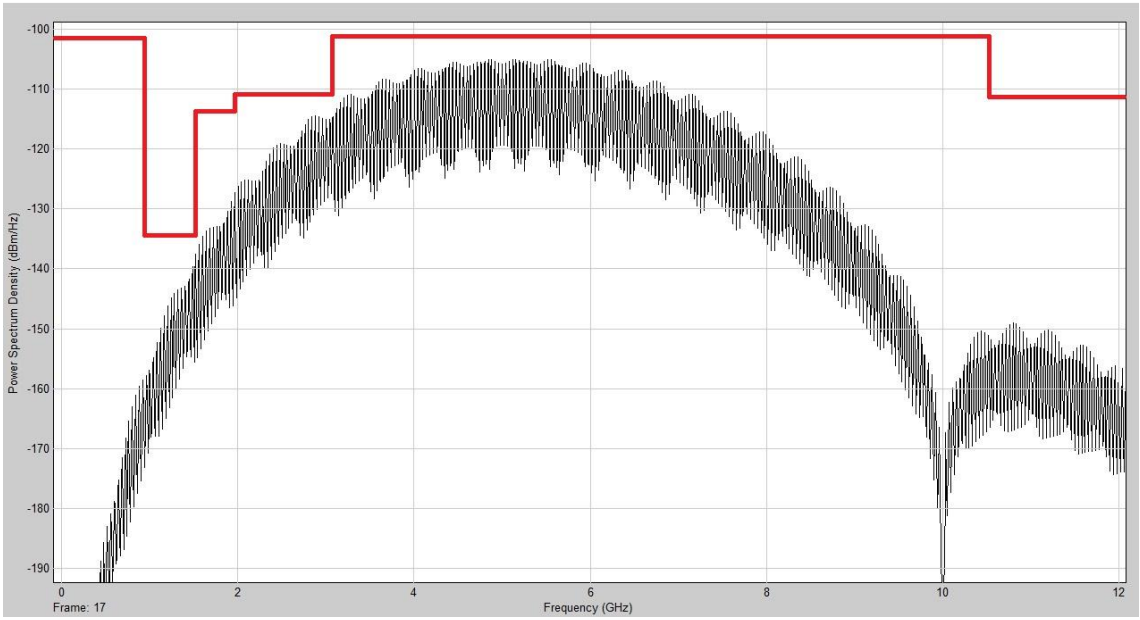

Fig.4. 9.Power spectral density of the transmitted S-OOK signal.

4.1.1.2. Radar mode

In the radar mode, a pulse is sent every bit time. Once again, that means all zeros for S-OOK or all ones for OOK. Fig 4.10 shows the waveform at the output of the transmitter.

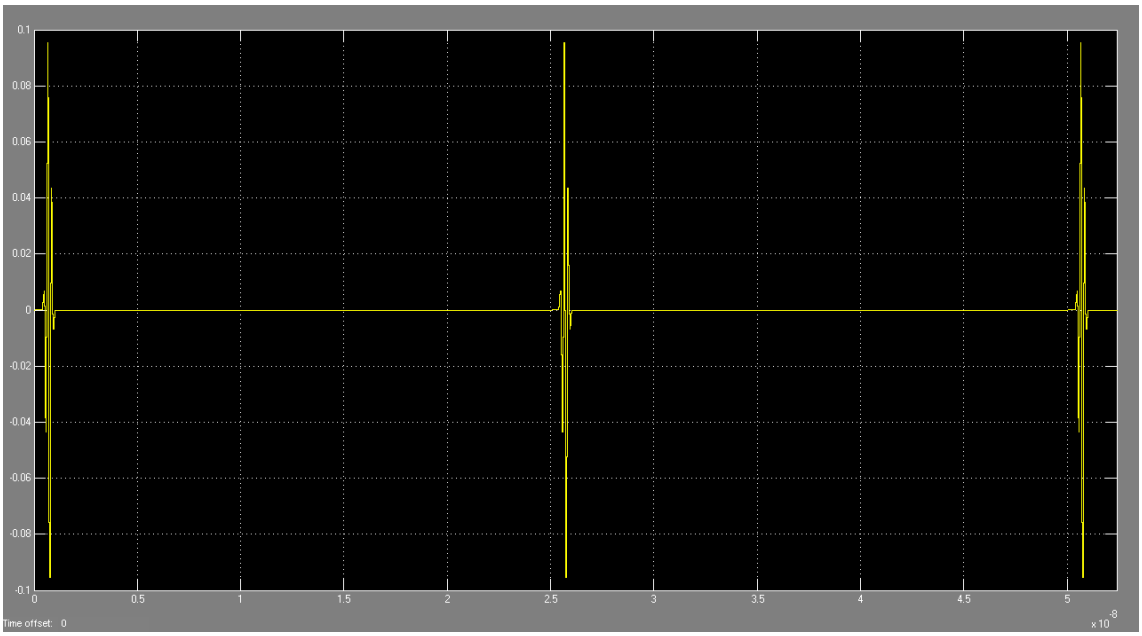

Fig.4. 10. RM's output of the transmitter in time domain

As it is a periodic signal, the harmonics are clearly seen in the PSD of Fig.4.11.

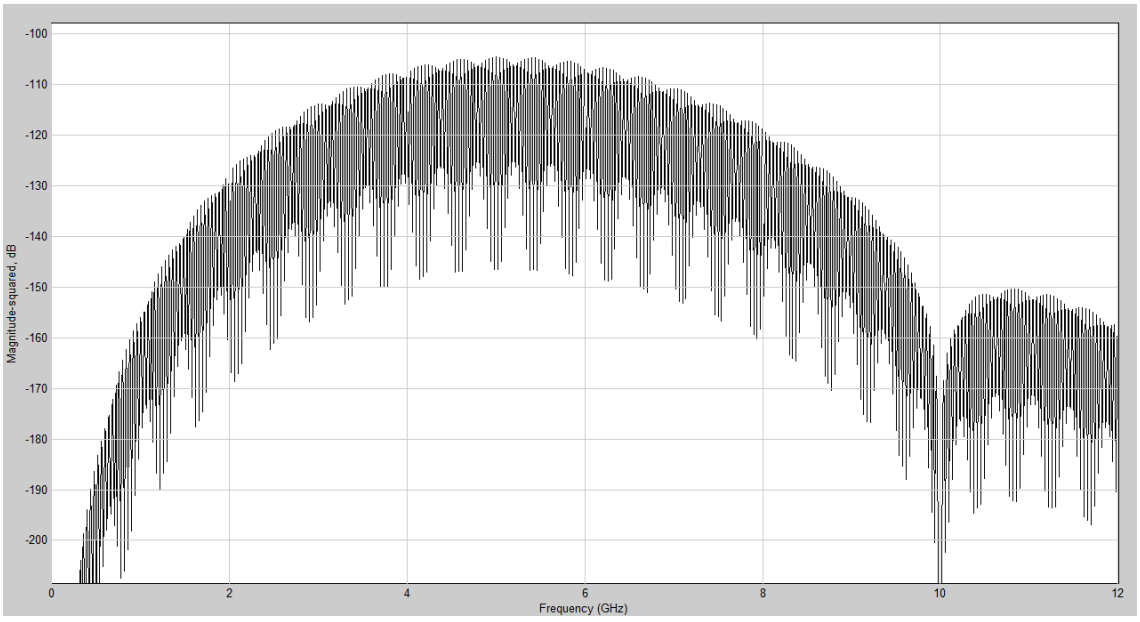

Fig.4. 11. RM's output of the transmitter in frequency domain.

4.1.2. Experimental Stage

As it was already introduced, in this stage only blocks from the Xilinx Blockset are used. Fig. 4.12, which contains the whole transmitter block's diagram with the indispensable System Generator's token, can be divided in three different parts: the Control MATLAB subsystem (top), the DC voltage susbsystem (bottom) and the transmitter itself with its two modes (middle).

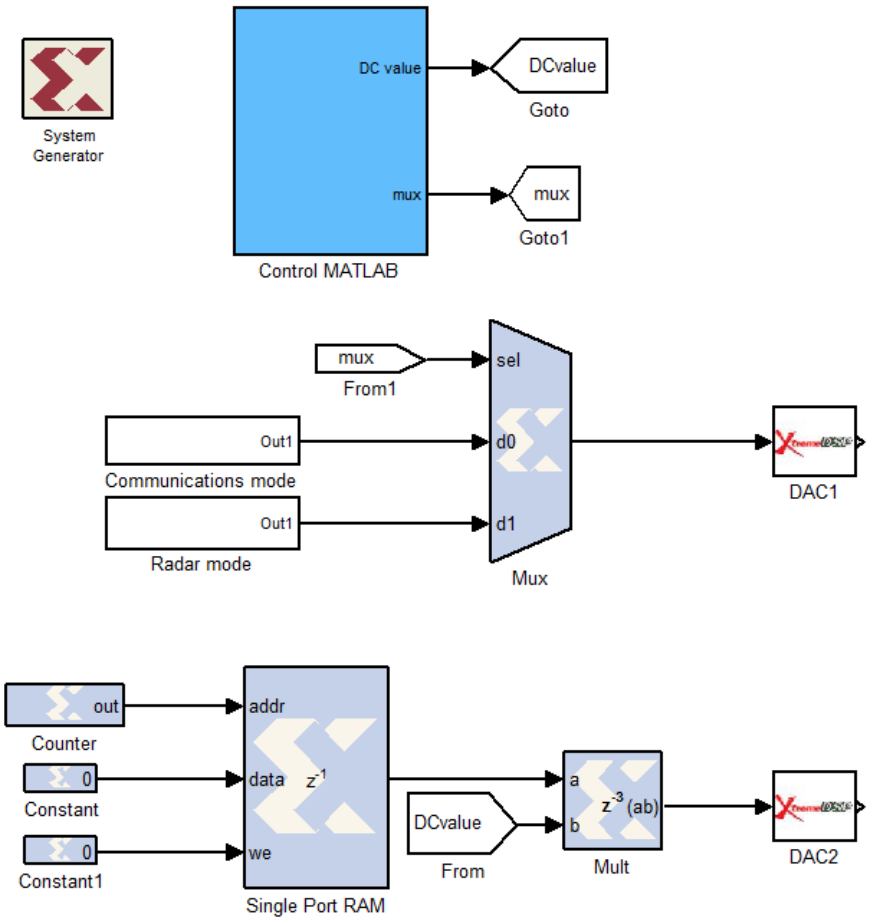

Fig.4. 12. Block diagram of the experimental transmitter.

Since the system in Fig. 4.12 has to be compiled and generated to be loaded in the FPGA, the only option to make modifications while the program is running is the Shared Memory. It allows changing some parameters through MATLAB during the execution. From MATLAB, a chain of bits is loaded in the Shared Memory and, with the BitBasher, the bits are properly divided with the desired data type thanks to the Convert. In Fig. 4.13, the implementation of Control MATLAB is shown. The subsystem has two outputs: "DC value" and "mux".

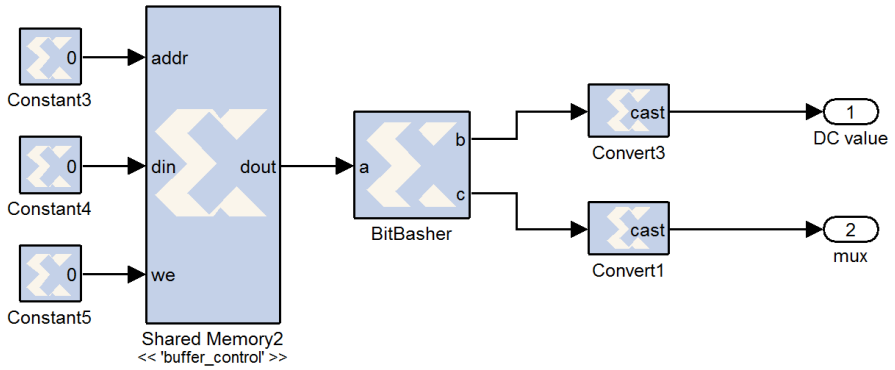

Fig.4. 13. Block diagram of the CONTROL MATLAB subsystem.

The “DC value” output is used for having a DC voltage with that value in volts at the output of DAC2. The DC voltage is connected to one of the V_{ctrl} inputs of the pulse generator explained in section 1.5 [10].

The “mux” output allows switching between the two operations modes: communications and radar.

4.1.2.1. Data transmission mode

The subsystem, shown in Fig. 4.14, is aimed at providing the S-OOK pulses that will trigger the pulse generator.

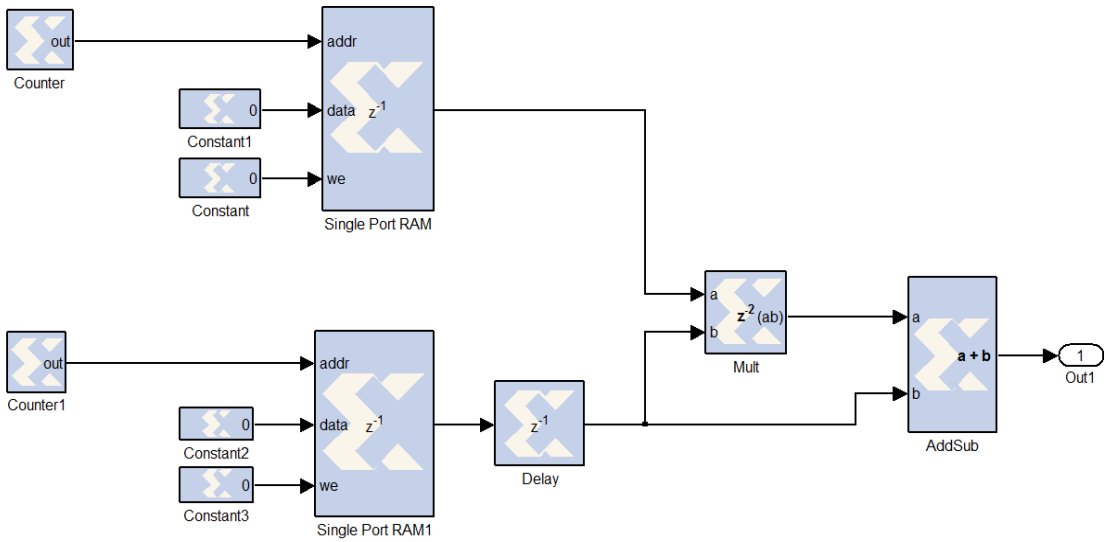

Fig.4. 14.Block diagram of the S-OOK data transmission mode subsystem.

Once more, the only difference between S-OOK and OOK is the presence of the synchronization pulse. In both cases, the random data is loaded in a Single

Port RAM, which puts one bit at its output every sample time. The other Single Port RAM is the one putting the synchronization pulse before each data pulse.

The signal is driven to the DAC1, where its waveform is the one shown in Fig. 4.15. For OOK each pulse represent one data bit while, for S-OOK, each two pulses are one data bit. As the converter is working at its maximum sampling rate, the signals are not as smooth as could be expected. DAC1 is connected to pulse generator and its waveform at the output is similar to the one in Fig. 4.16.

Fig.4. 15. OOK (top) and S-OOK (bottom) communications signal's waveform at the output of DAC1.

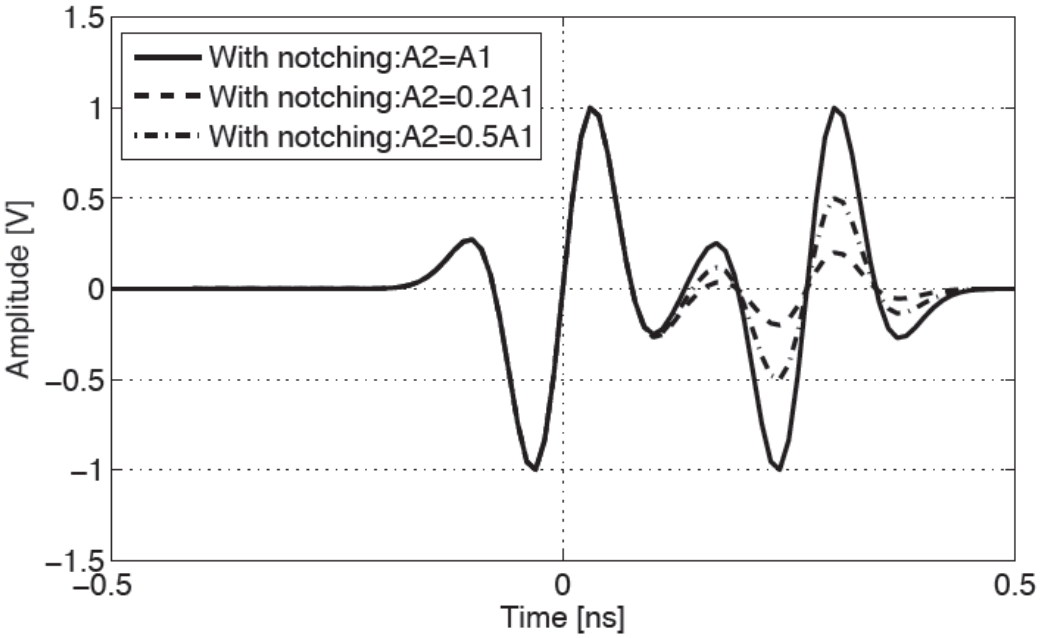

Fig.4. 16. Pulse waveform at the output of the pulse generator [10].

Fig. 4.17 and 4.18 show the PSD of the OOK and S-OOK signal at the output of the pulse generator, respectively. As discurssed before, the number of pulses per bit is lower for OOK than for S-OOK. Therefore, the PSD reaches higher values in the second case.

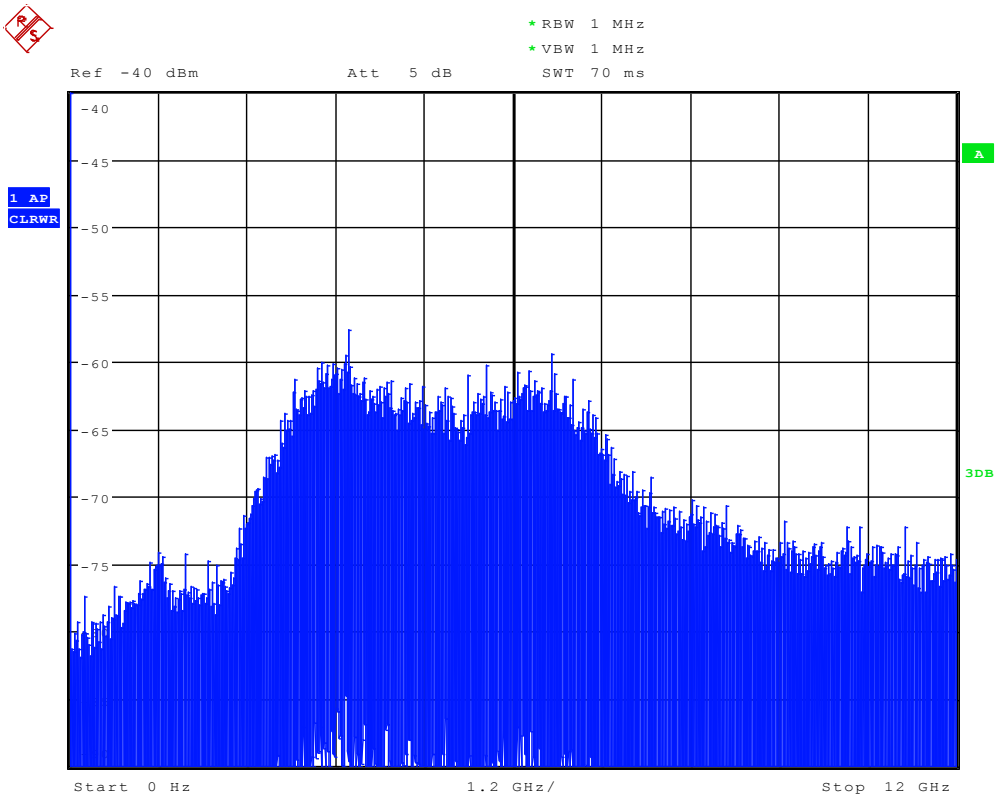

Fig.4. 17. PSD of the OOK signal.

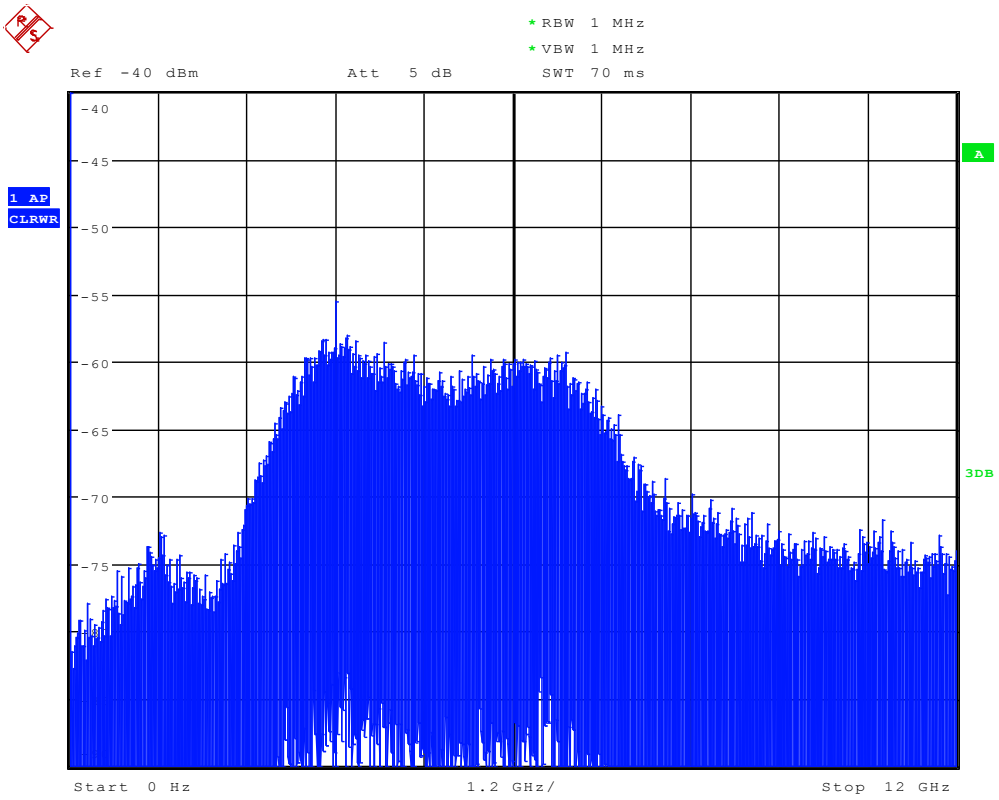

Fig.4. 18. PSD of the S-OOK signal.

In both cases the signal is way below the FCC mask so there is still room to amplify it and/or increase the data rate (a faster DAC would be needed).

4.1.2.2. Radar mode

The implementation of the radar mode consists in a Single Port RAM whose output changes from 1 to 0 every sample time (See Fig 4.19).

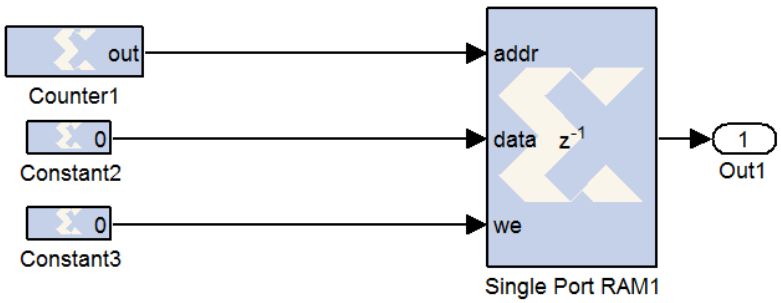

Fig.4. 19. Block diagram of the radar mode subsystem.

That signal is driven to the DAC1 and the time-domain resulting signal can be seen in Fig. 4.20.

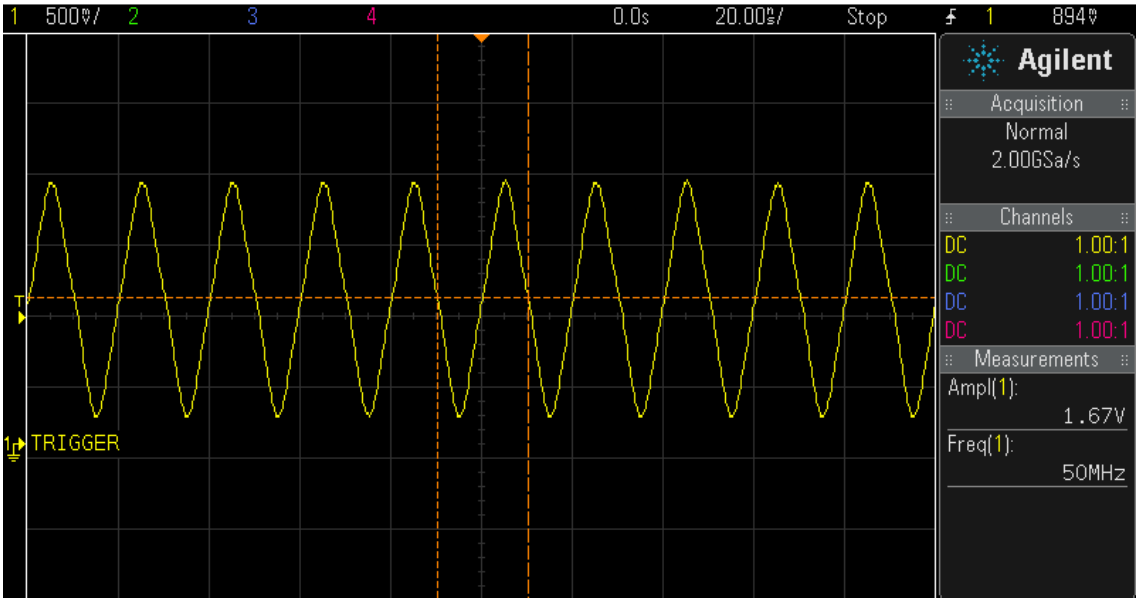

Fig.4. 20. Radar signal's waveform at the output of DAC1.

The spectrum of the signal at the output of the pulse generator is shown in Fig. 4.21. As it is a periodic signal, all the harmonics can be seen, while in the data mode, the spectrum was much more continuous.

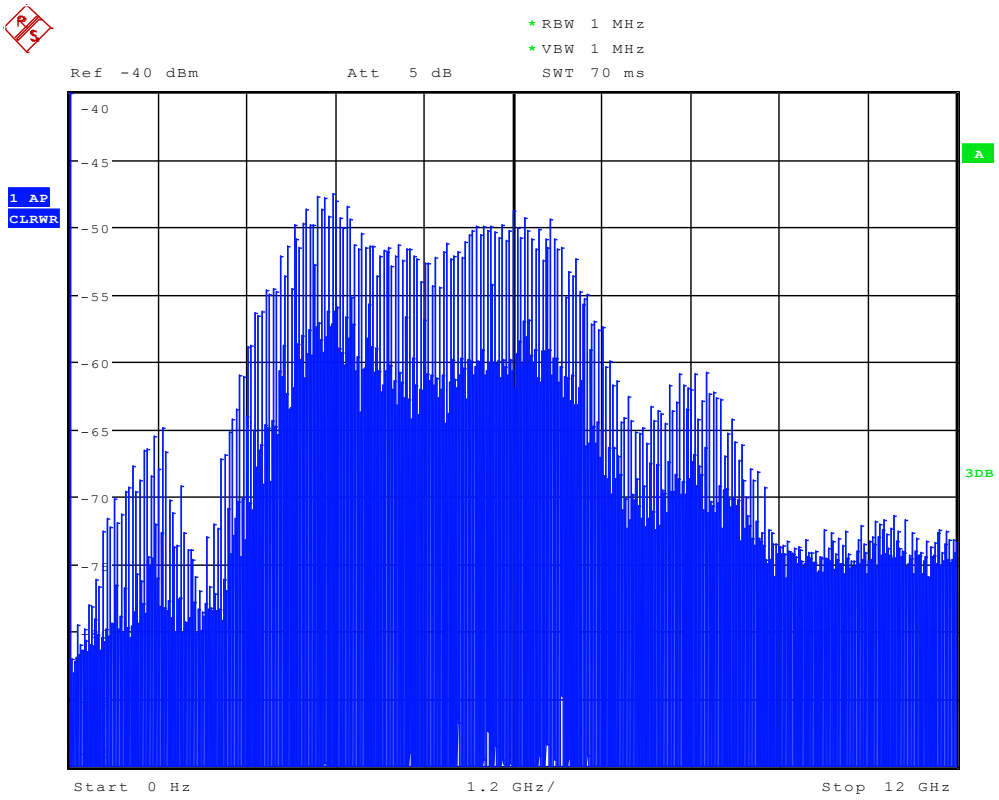

Fig.4. 21. Radar signal's PSD at the output of the pulse generator.

4.2. Channel modeling

Both operation modes must face the effects of the channel. The main effects are the path loss, multipath propagation. However, these effects are different for each mode.

The path loss in DTM is mainly due to free-space propagation, while in RM, the different dielectric properties of each organ or tissue must have a great impact in the signal attenuation.

The multipath replicas of the signal in DTM are usually undesired because they can cause destructive interference. Nonetheless, in RM, the reflections are used to measure the desired parameter.

These differences are the reason why the channels for DTM and RM were modeled independently. Even so, the addition of thermal noise to the signal is common for both cases. The next two subsections show the modeling for each mode.

4.2.1. Data transmission mode

For this first approach, the DTM channel is aimed at being able to set a certain Signal-to-Noise Ratio (SNR) at its output. Future versions may include a more realistic channel model such as the Modified Saleh Valenzuela [24]. The basic channel model used is shown in Fig. 4.22.

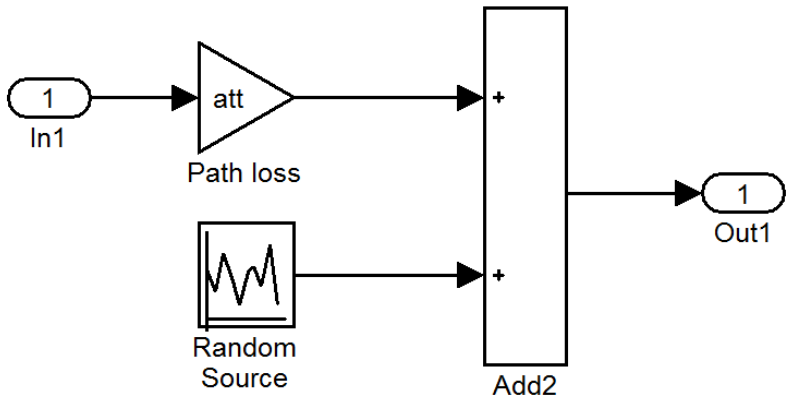

Fig.4. 22. DTM channel model's block diagram.

The transmitted signal is attenuated and, then, the thermal noise is added. This Additive White Gaussian Noise (AWGN) has a power density of -174 dBm/Hz, as it can be seen in Fig.4.23.

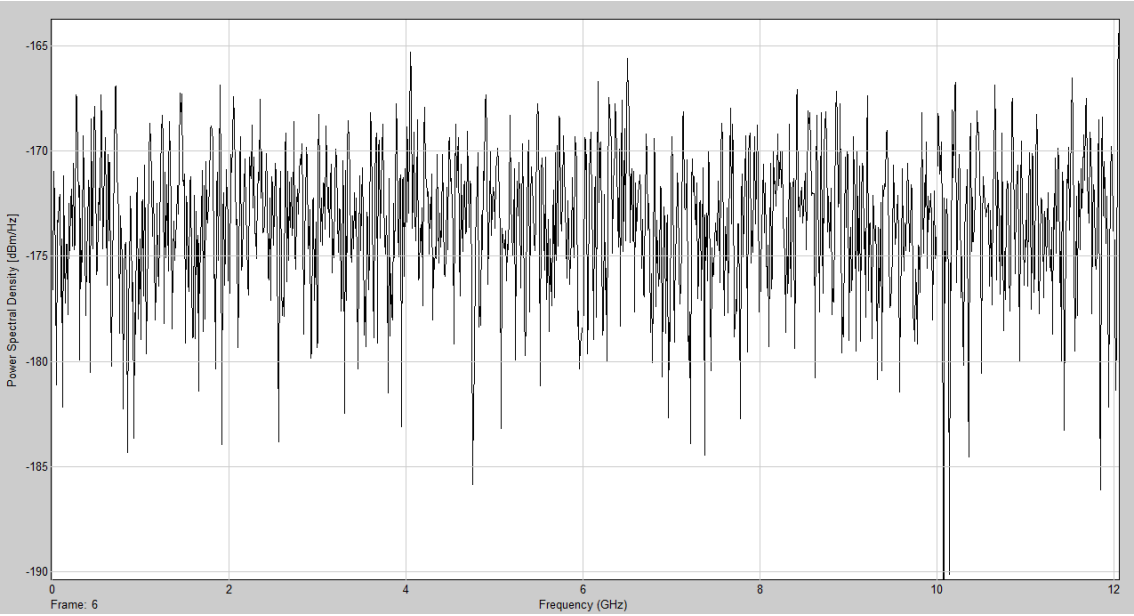

Fig.4. 23.Thermal noise PSD

The value for the path loss is set in a way that the desired SNR is achieved. The SNR is defined as:

$$SNR = \frac{P_o}{P_n} = \frac{V_o^2}{V_n^2} \quad \textbf{(4.5)}$$

As the goal is obtaining the factor by which the transmitted signal's amplitude must be attenuated, the output voltage of equation 4.5 has to be substituted by the input voltage times the attenuation factor (V_o = att · V_i). Then, isolating the attenuation factor, one obtains:

$$att = \sqrt{SNR \cdot \frac{P_n}{P_i}} \quad \textbf{(4.6)}$$

It is important to remark that the noise power (P_n) must be calculated considering the bandwidth of the signal. For the simulations carried out, the 3-dB-bandwidth of the signal was found to be 2.5 GHz. Therefore:

$$P_n(dBm) = -174\ dBm/Hz + 10 \log BW_{3dB} \quad \textbf{(4.7)}$$

Fig. 4.24 shows the waveforms of the input signal, the noise and their addition, which is the output signal. As the SNR decreases, the signal is more attenuated until it is finally hidden by the noise.

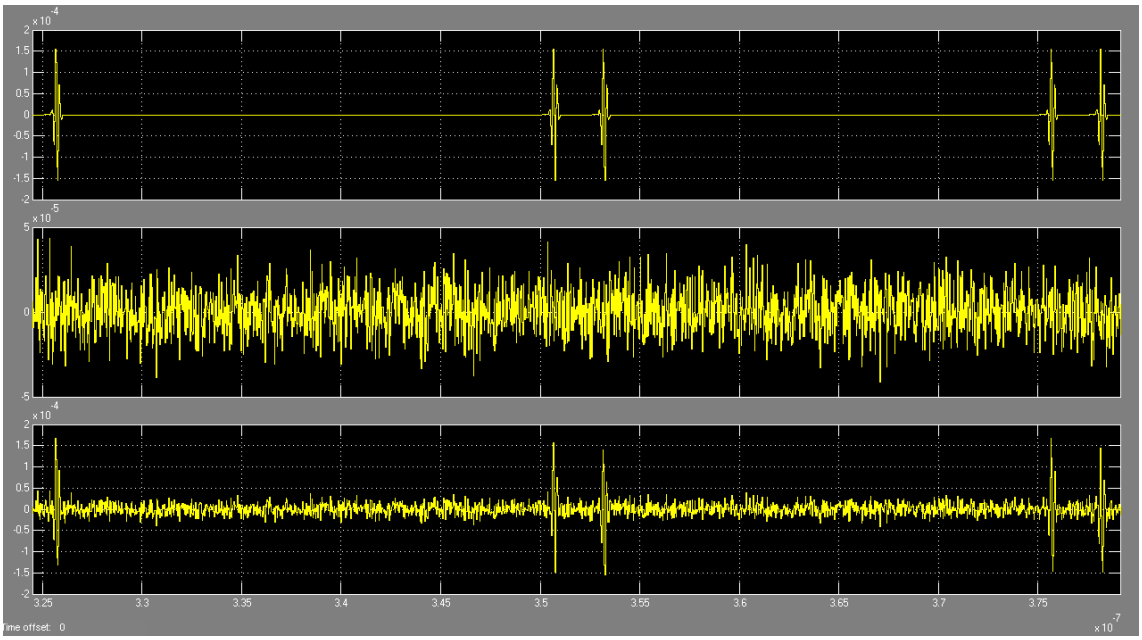

Fig.4. 24. Input signal, noise and output signal in the time domain.

The PSD of the signal at the output of the Channel block, i.e. at the input of the receiver, can be seen in Fig. 4.25.

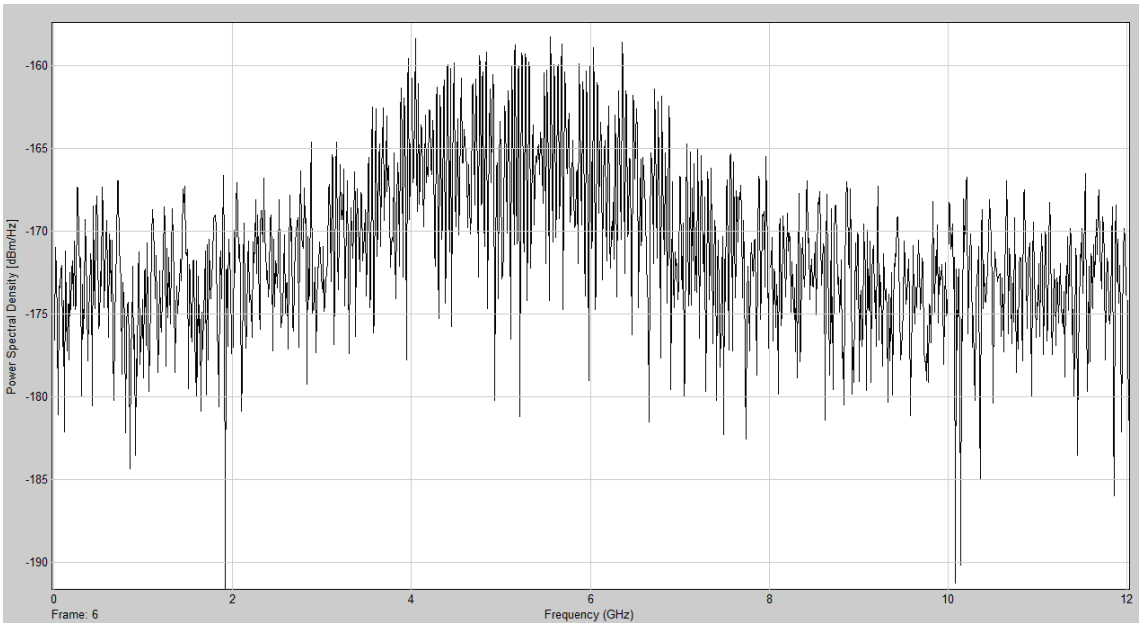

Fig.4. 25. Output signal in the frequency domain.

4.2.2. Radar mode

In this work, the RM is aimed at monitoring the urine accumulation in the bladder. The first approach is to model the RM channel only taking into account the delay and the attenuation affecting the pulses. Several simplifications have been done to have a simple, but still realistic, model.

By taking [26] as a reference, two arrangements have been considered for doing the measurements: transmission and reflection. They are depicted in Fig 4.26. The transmission arrangement is just for testing purposes since having the patient between the two antennas is not a practical solution. The measured target is simplified to one layer of a material with a certain thickness and relative permittivity.

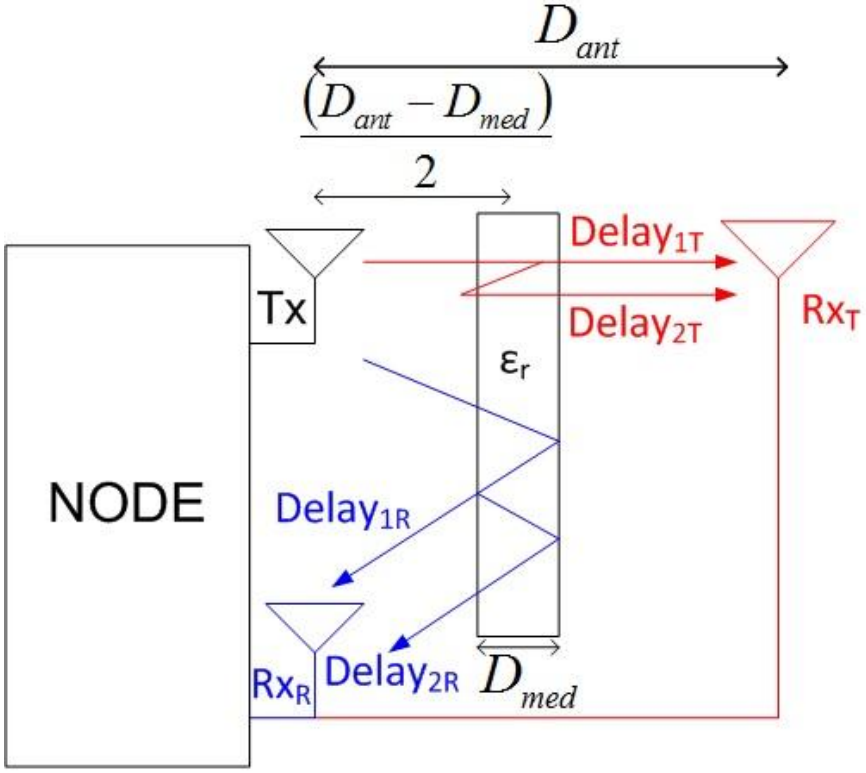

Fig.4. 26. Transmission (red) and reflection (blue) arrangements for the RM.

The equations for modeling the time delays are based on the ones used in [26]. The frequency dependency of the phase constant and the transmission and reflection losses and angles have not been considered. The delays only depend on the distance between the antennas (D_{ant}), the thickness of the medium (D_{med}), the relative permittivity of the medium (ε_r) and the speed of light in vacumm (C_o). Below are the equations for the delays in each arrangement.

$$v_{med}[m/s] = \frac{C_o}{\sqrt{\varepsilon_r}} \quad \textbf{(4.8)}$$

$$Delay_{1T}[s] = \frac{D_{ant} - D_{med}}{C_o} + \frac{D_{med}}{v_{med}} \quad \textbf{(4.9)}$$

$$Delay_{2T}[s] = Delay_{1T} + 2 \cdot \frac{D_{med}}{v_{med}} \quad \textbf{(4.10)}$$

$$Delay_{1R}[s] = \frac{D_{ant} - D_{med}}{C_o} + 2 \cdot \frac{D_{med}}{v_{med}} \quad \textbf{(4.11)}$$

$$Delay_{2R}[s] = Delay_{1R} + 2 \cdot \frac{D_{med}}{v_{med}} \quad \textbf{(4.12)}$$

On the other hand, the equations modeling the attenuations are based on the ones proposed in [27], where the attenuation constant for a lossy dielectric material is defined as:

$$\alpha(\omega)[Np/m] = \frac{\omega}{C_o}\sqrt{\frac{\varepsilon_r}{2}\left(\sqrt{1+p_e^2}-1\right)} \quad \textbf{(4.13)}$$

$$p_e = \tan\delta + \frac{\sigma}{\omega\varepsilon_r\varepsilon_o} \quad \textbf{(4.14)}$$

In which, $\omega = 2\pi f$ and p_e is the effective loss tangent of the material, which depends on its loss tangent ($\tan\delta$), its conductivity and its absolute permittivity ($\varepsilon_r\varepsilon_o$). For simplification, the attenuation is considered constant for the whole bandwidth by doing the calculations with f = 3.9 GHz. The material considered for the simulations is urine and the needed parameters are obtained from [28]. For more realistic models, more layers representing the human tissues and organs must be added. The dielectric parameters for those layers can be found in [29][30][31].

Nevertheless, the attenuation is not only because of the medium, there is also free-space propagation thus free-space path loss (FSPL). For taking it into account, the equation 4.15 has been applied. It is not accurate, since it is for the far-field region, but it is enough for this first characterization. In both arrangements the distance is D_{ant} - D_{med}.

$$FSPL = \left(\frac{4\pi df}{c_o}\right)^2 \quad \textbf{(4.15)}$$

Therefore, the attenuations for the two pulses are calucated as follows:

$$att_{1T} = \frac{1}{\sqrt{FSPL}}e^{-\alpha\cdot D_{med}} \quad \textbf{(4.16)}$$

$$att_{2T} = \frac{1}{\sqrt{FSPL}}e^{-\alpha\cdot 3\cdot D_{med}} \quad \textbf{(4.17)}$$

$$att_{1T} = \frac{1}{\sqrt{FSPL}}e^{-\alpha\cdot 2\cdot D_{med}} \quad \textbf{(4.16)}$$

$$att_{2T} = \frac{1}{\sqrt{FSPL}}e^{-\alpha\cdot 4\cdot D_{med}} \quad \textbf{(4.17)}$$

Once the parameters are calculated, they are introduced in their respective Simulink blocks seen in Fig.4.27. As it is a sample-based simulation, the delays are introduced by rounding the quotient between the calculated delay and the simulation step.

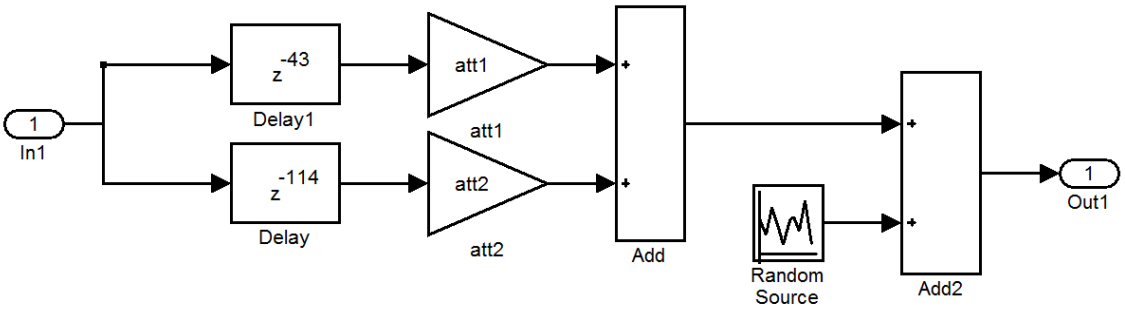

Fig.4. 27. RM channel model's block diagram.

By looking at the equations, one can notice that the difference between the two arrangements is that both the delays and the attenuations are larger for the reflection case. Fig. 4.28 shows the waveforms of each reflection and their addition. Note that the second reflection is about two orders of magnitude smaller than the first one. This is why just two reflections were considered.

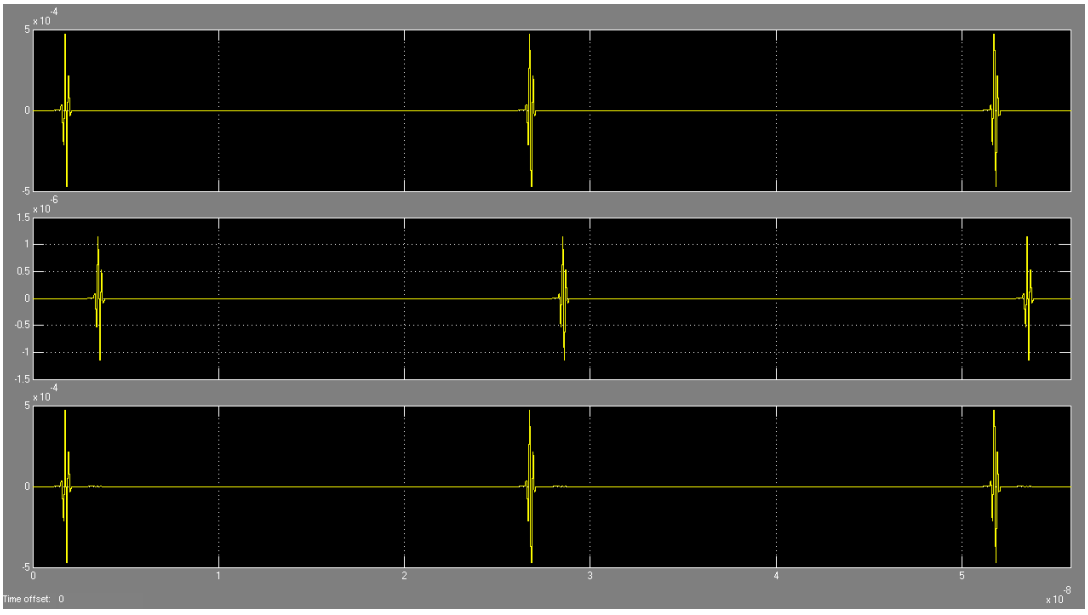

Fig.4. 28. Breakdown of the reflected pulses.

Having such a weak signal is not desirable because the noise may hide the reflections as happens in Fig. 4.29. Even so, this can be solved by correlating the signal at the receiver side. As the noise is uncorrelated, the reflections will be seen.

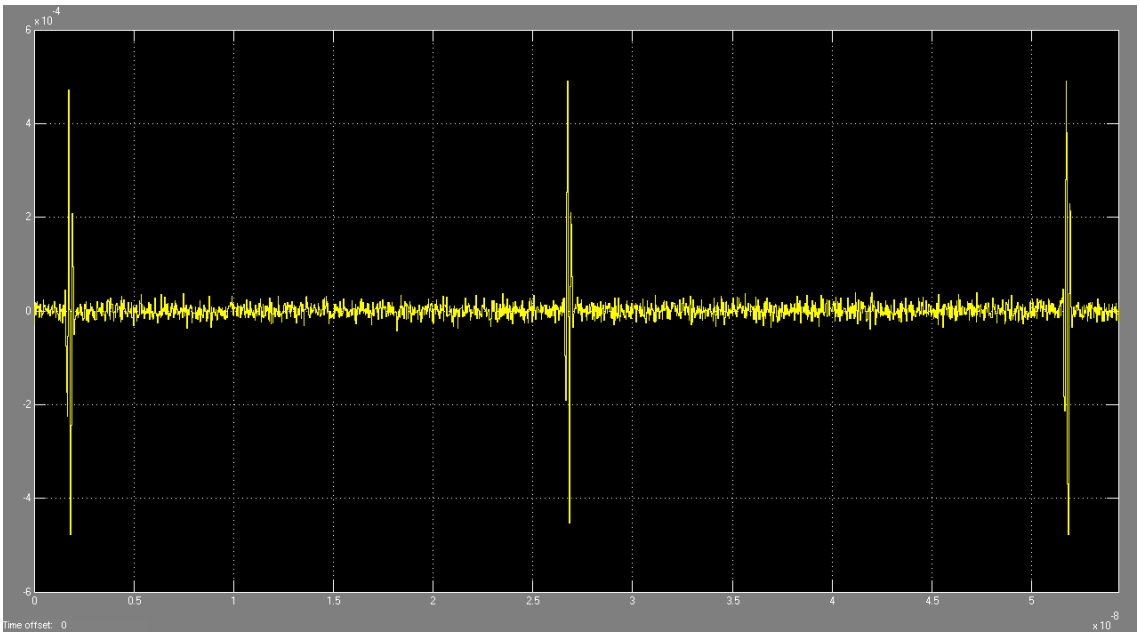

Fig.4. 29. Signal's waveform at the receiver in RM.

4.3. Receiver

The receiver of this work has been implemented using the Energy Detection (ED) scheme for the demodulation of the signal, and Equivalent-Time Sampling (ETS) to sample the signal. ETS is a common technique for both modes of operation, while ED is only used in the DTM. Both techniques are explained in-depth below:

Energy detection

A variety of receiver's architectures have been studied to carry this work out [23] [32]. The most important ones are Correlation-based (CB) receivers and ED receivers.

The CB receivers demodulate the signal after doing a correlation between the received signals and a template of the transmitted signal. This kind of receivers needs a really accurate timing to generate the template and do the correlation thus synchronization is needed. The main disadvantage of this type of receiver is that if the signal is very noisy, the receiver is not able to detect the reference pulse when correlates it with the template.

ED receivers' structure is typically used when the modulation is a non-coherent one like OOK [32]. The main difference between the CB receivers and the ED ones is that the second ones do not require synchronization to recover the transmitted information. A general scheme of an ED receiver is shown in Fig. 4.30.

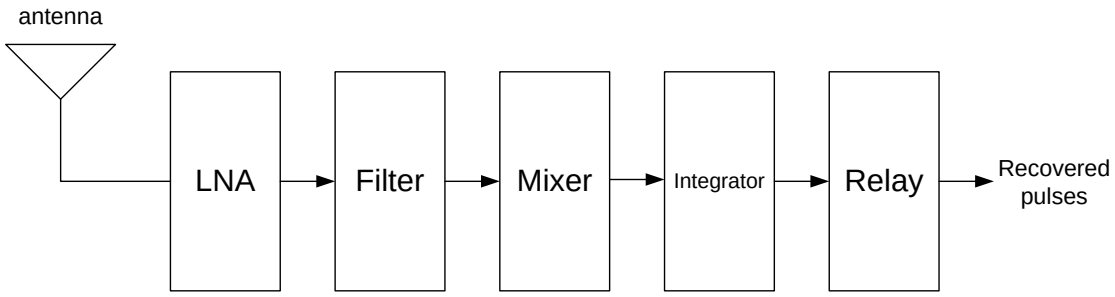

Fig.4. 30. General diagram for the Energy Detector Receiver

.

As the DTM of this work uses S-OOK, this ED receiver structure is also able to recover the data and the clock of the signal. The method is explained in [23]. One of the main difficulties of this kind of receiver is finding the optimal threshold for the Relay block (Fig. 4.30). In this work, a fixed thershold has been use. However, the optimum solution would have been the implementation of an adaptive threshold that would have improved the BER performance of the system.

Equivalent-time sampling

There are two sampling methods that can be use to recover a signal, Real-time sampling (RTS) and Equivalent-time sampling (ETS).

RTS captures all samples with one triggering signal (Fig. 4.31). The resolution of the recovered signal depends only on the sampling rate of the ADC and the number of bits.

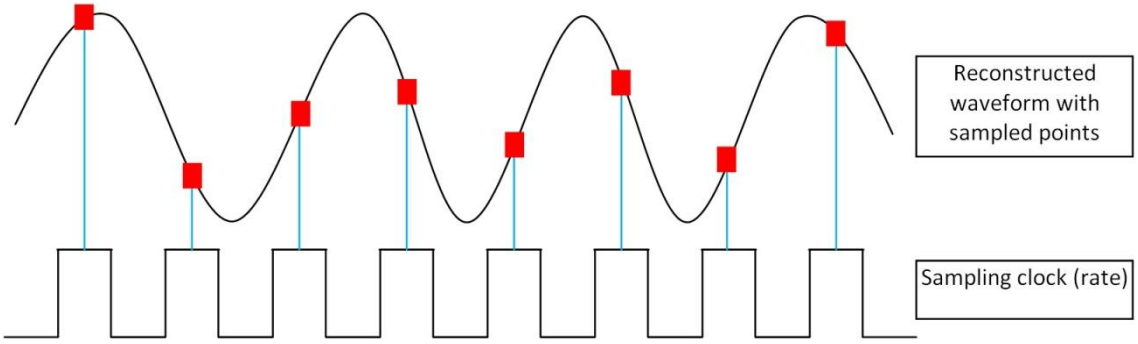

Fig.4. 31. Real time sampling method [33]

On the other hand, ETS is very useful when the sampling rate of the converter is not high enough. The UWB pulses used in this work are very narrow (in the order of ns) and the system frequency due these narrow pulses is very high (in the order of GHz). Therefore, the needed sampling frequency is also really high. As the ADCs with a high sampling rate are very expensive and keeping the cost

as low as possible was an objective of this work, ETS has been the selected sampling method.

In ETS, the recovered signal is sampled using multiple triggering signals at different clock timing; there is a phase difference between every sampling time that makes the sampling instant change every acquisition time. Then the signal is rebuilt using the samples acquired from each acquisition and put it all together. If the phase-shifting step is narrower, the reconstruction of the signal will be better. This means better resolution thus better system performance. Nevertheless, ETS cannot be used for capturing signals that are not periodic. Fig 4.32 illustrates how ETS works.

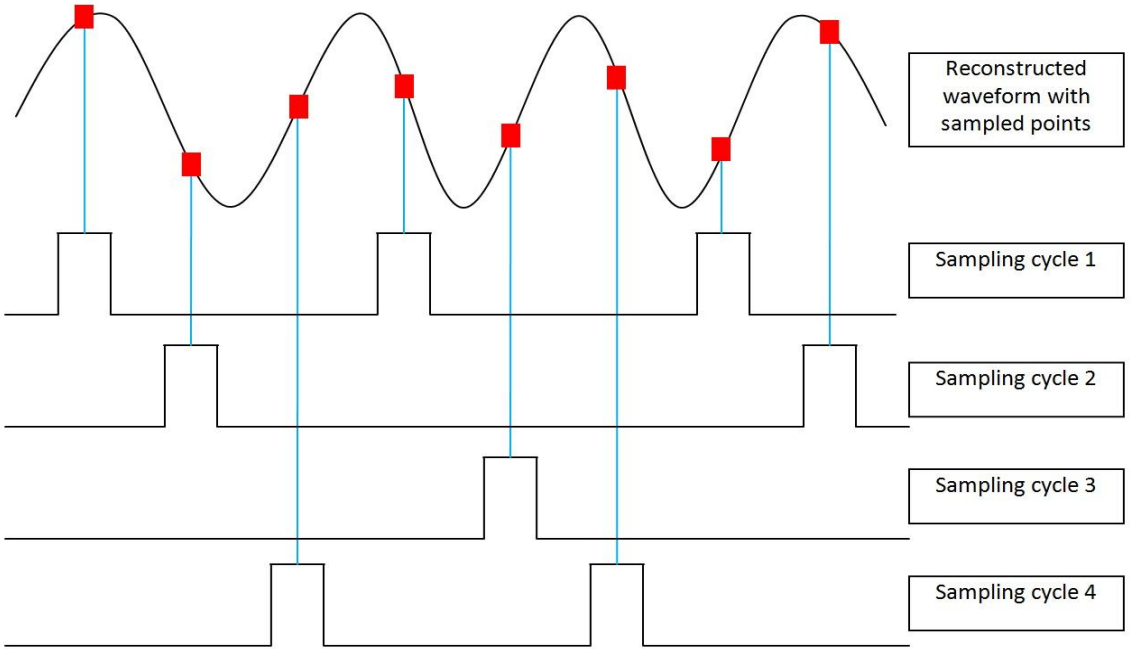

Fig.4. 32.Equivalent-time sampling method [33]

There are two kinds of ETS methods, random ETS (R-ETS) and sequence ETS (S-ETS) [34].

In the R-ETS method, the phase difference between two adjacent sampling times is following a random distribution. This kind of ETS is more complicated to implement because it needs a reference point to reconstruct the signal.

In the S-ETS method, the phase difference between two adjacent sampling clocks is constant. Therefore, it is easier to implement because the collected samples are in order and there is no need to reorganize them.

For this work, S-ETS has been designed with Simulink®. Fig. 4.33 shows the block diagram of the implementation. Because of a lack of RAM memory in the computers used for running the simulation, no results with the ETS system

integrated were obtained. This is due to the extremely high number of samples needed to reconstruct each pulse in the simulation platform designed.

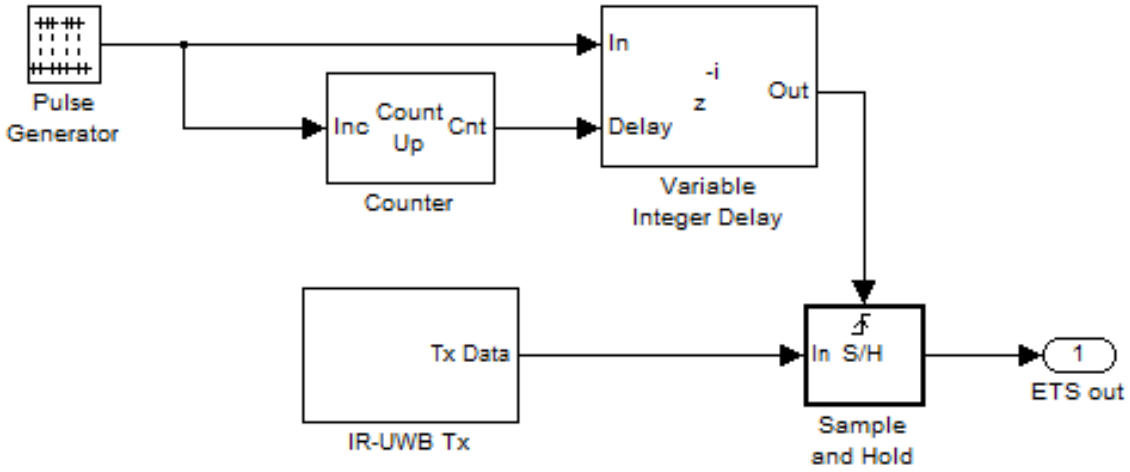

Fig.4. 33. Block diagram of the ETS implemented system.

As it is said before, ETS is not useful for capturing non-repetitive signals. To allow its use for the DTM, the transmitter must keep on sending the same bit as many times as the ETS receiver's block needs to reconstruct the signal. That means making the signal periodic during a certain time. However, there is a trade-off between the bit rate and the BER. The number of repetitions in the transmitted pulse must guarantee a sufficient reconstruction and assure an enough bit rate for the application. In Fig.4.33 a pulse generator that generates the trigger to sample the pulses could be seen. Then the Variable Integer Delay adds the phase shift to each one of the triggers. This phase shift is controlled by a counter. The counter counts one by one during the number of samples of the ETS, and tells the Variable Delay which is the delay for each triggering pulse. Then, the Sample and Hold is controlled by the rising edge of phase-shifted triggered pulses, while the input signal is the pulses generated by the IR-UWB block. The results are shown below. In the Fig.4.34 could be seen how a '0' and a '1' are recovered. Waveforms 1 and 2 are the triggers and the pulses that would be recovered respectively.

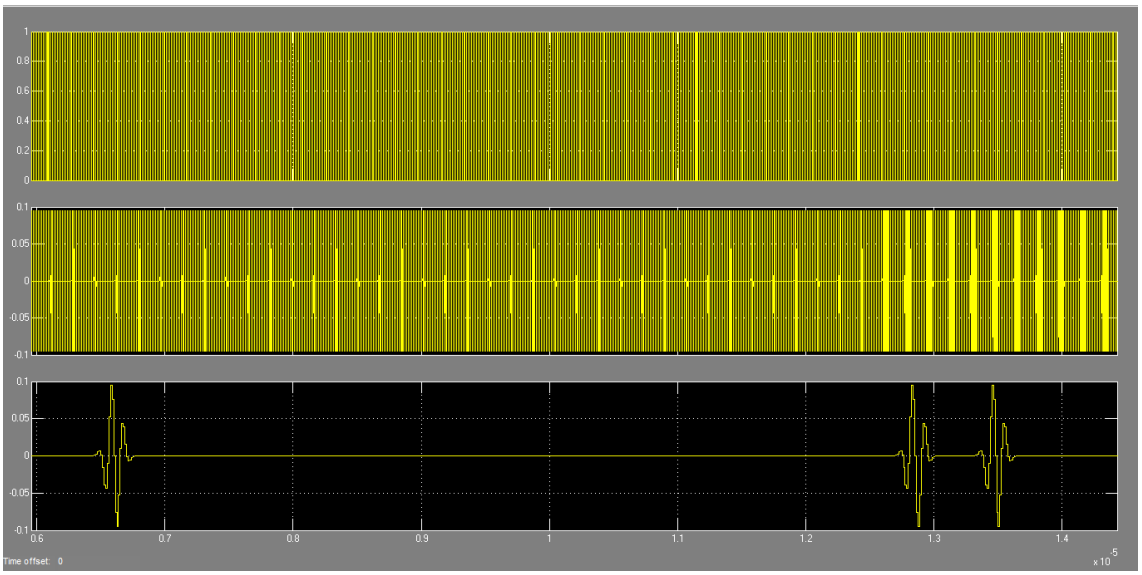

Fig.4. 34. ETS system results Data transmission mode time domain

Because every output pulse is generated by samples of small pulses it is impossible to see both pulses in one graph. In the figure below a zoom of the trigger generated by the pulse generator and the periodic pulses is done to show how ETS is working.

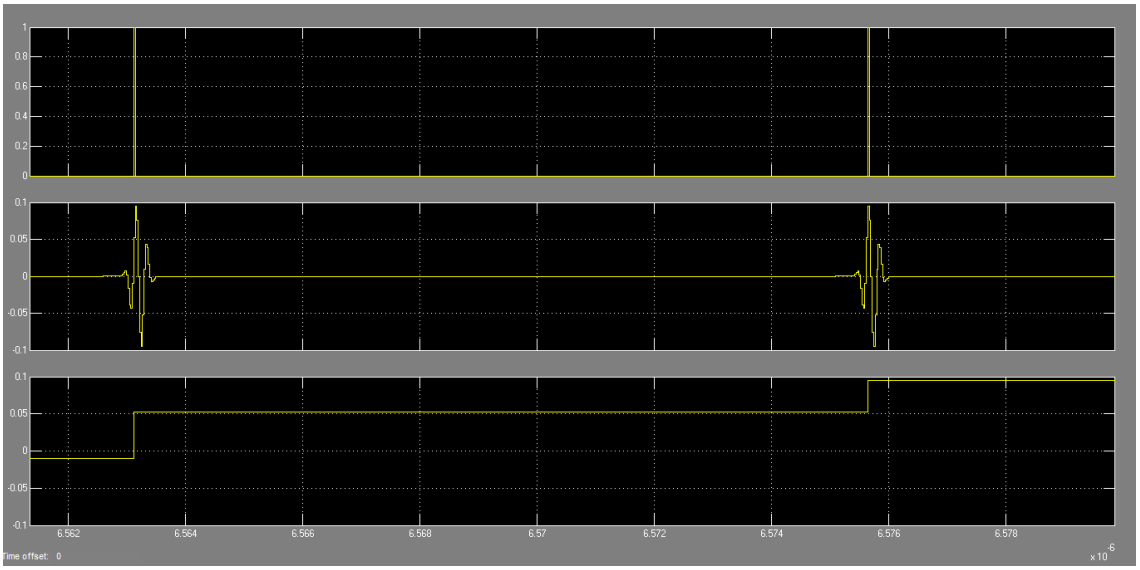

Fig.4. 35. ETS system results Data transmission mode zoom in time domain.

It could be seen in Fig. 4.35 that every trigger (waveform 1) takes a different value of the pulse, and is held while not reaching the next trigger. This process is how the signal is reconstructed.

This simulation is made using Data transmission mode, but the ETS also works with Radar mode. In the case of the Radar mode a lot of copies of the pulse are

not nedeed to make the signal periodic, because the Radar mode signal is also a periodic signal and works properly with ETS.

Once the techniques used for both modes of operation had been explained, next subchapters are going to show the simulated results for each one of the modes.

All the results shown of the receiver will be simulations because we were not able to obtain experimental results. The main reason is because the ADCs of our XtremeDSP Development kit for Virtex-4 (AD6645 from Analog Devices) had an analog input bandwidth of 270 MHz. The analog bandwidth is the analog input frequency for which the spectral power of fundamental frequency is reduced by 3 dB. Our signals could be found between 3 GHz and 10 GHz, so the ADCs analog bandwidth is not enough to work with this kind of signals. The sampling frequency of the ADC is also low, 105 MHz, but this would not be a problem if we are able to use Equivalent-time sampling. A solution to obtain measured results was a UWB Radar kit from GEOZONDAS, like the one used in paper [26].The kit had been ordered but it arrived too late to include measured results in this report. These results are going to be show in the presentation.

Before showing the results of the simulations, an explanation of the receiver system will be done.

In Fig.4.36 can be seen the proposed solution for our receiver. As is told before, ETS method is needed and used for both common modes, while Energy detection is only used for the Data transmission mode. In this scheme the LNA, the filter and the ETS block are common blocks. The Data transmission mode is mostly composed by software element. Also the switch that controls the mode is software. This switch would be controlled automatically by the FPGA. But as it is shown before, the Data transmission mode using ETS needs a lot of samples to reconstruct the signal, which made this method really slow and not good for fast applications. For that reason an alternative receiver solution is proposed [Fig. 4.37]. In this solution the Radar mode is still the same as in the other solution, because ETS works properly with periodic signals. To solve the problem of ETS for fast applications, in Data transmission mode, our proposal is to use a real-time ADC because the frequency of the signal, after the Flip-Flop, is not that high. In this case most of the Data transmission mode is hardware. Also the switch that manages the two modes is hardware, but is still controlled automatically by the FPGA.

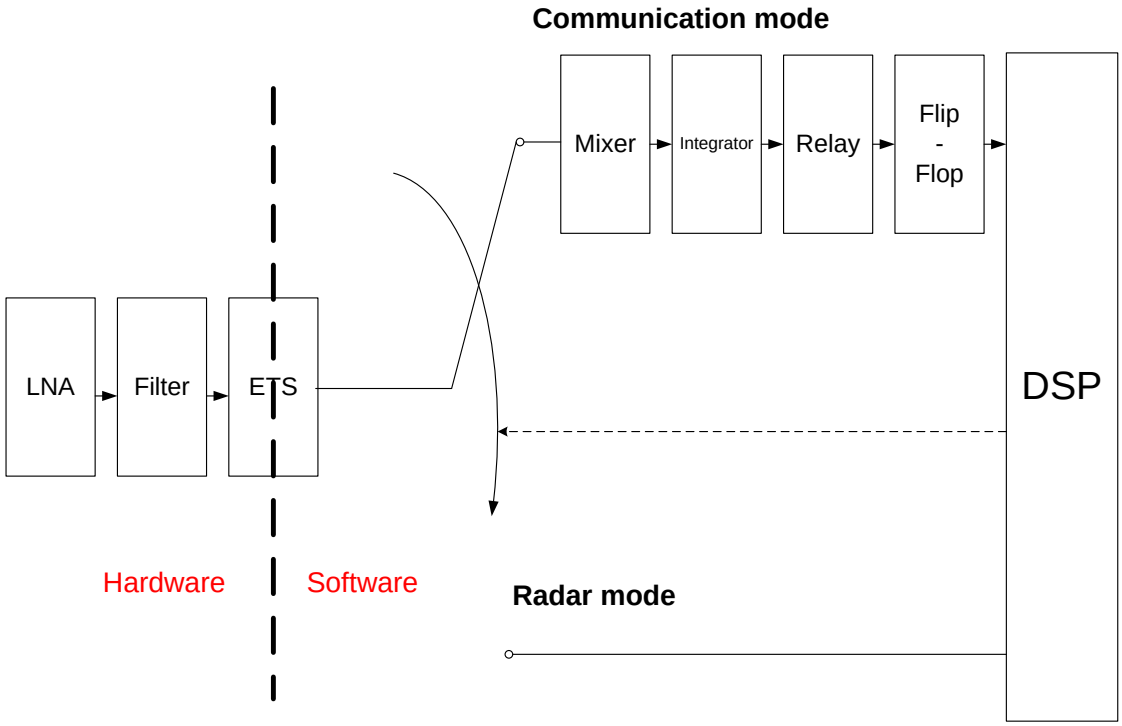

Fig.4. 36. Proposed receiver solution

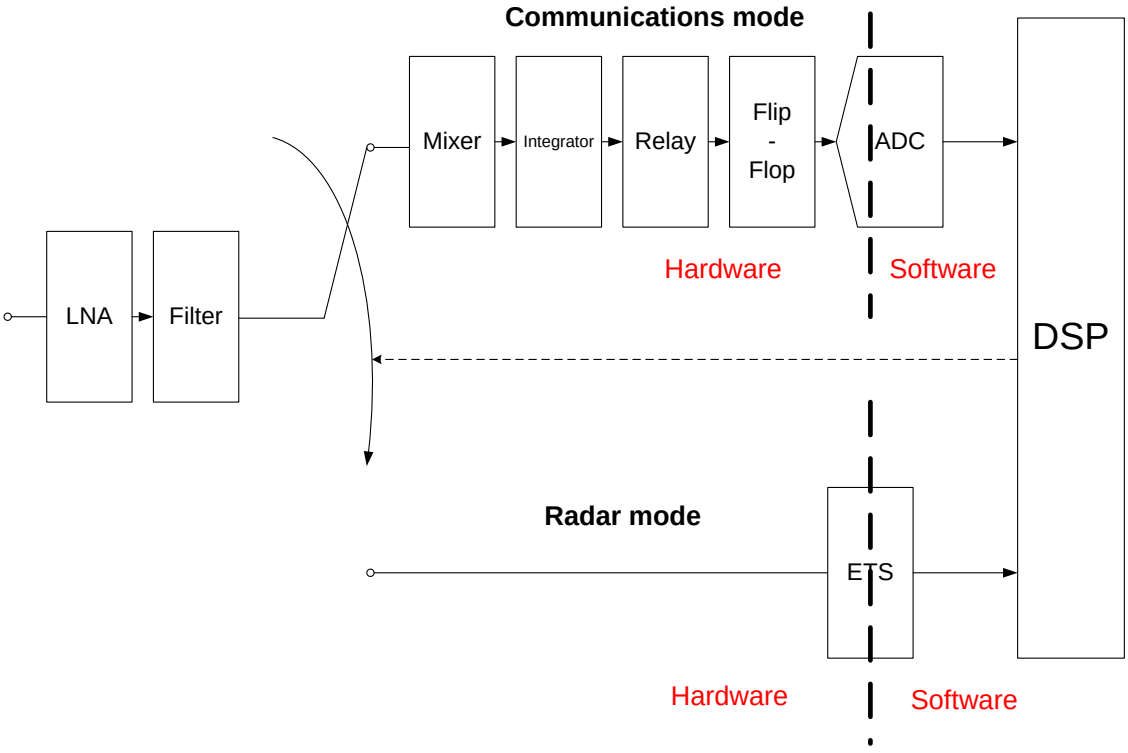

Fig.4. 37. Alternative receiver solution

4.3.1. Data transmission mode

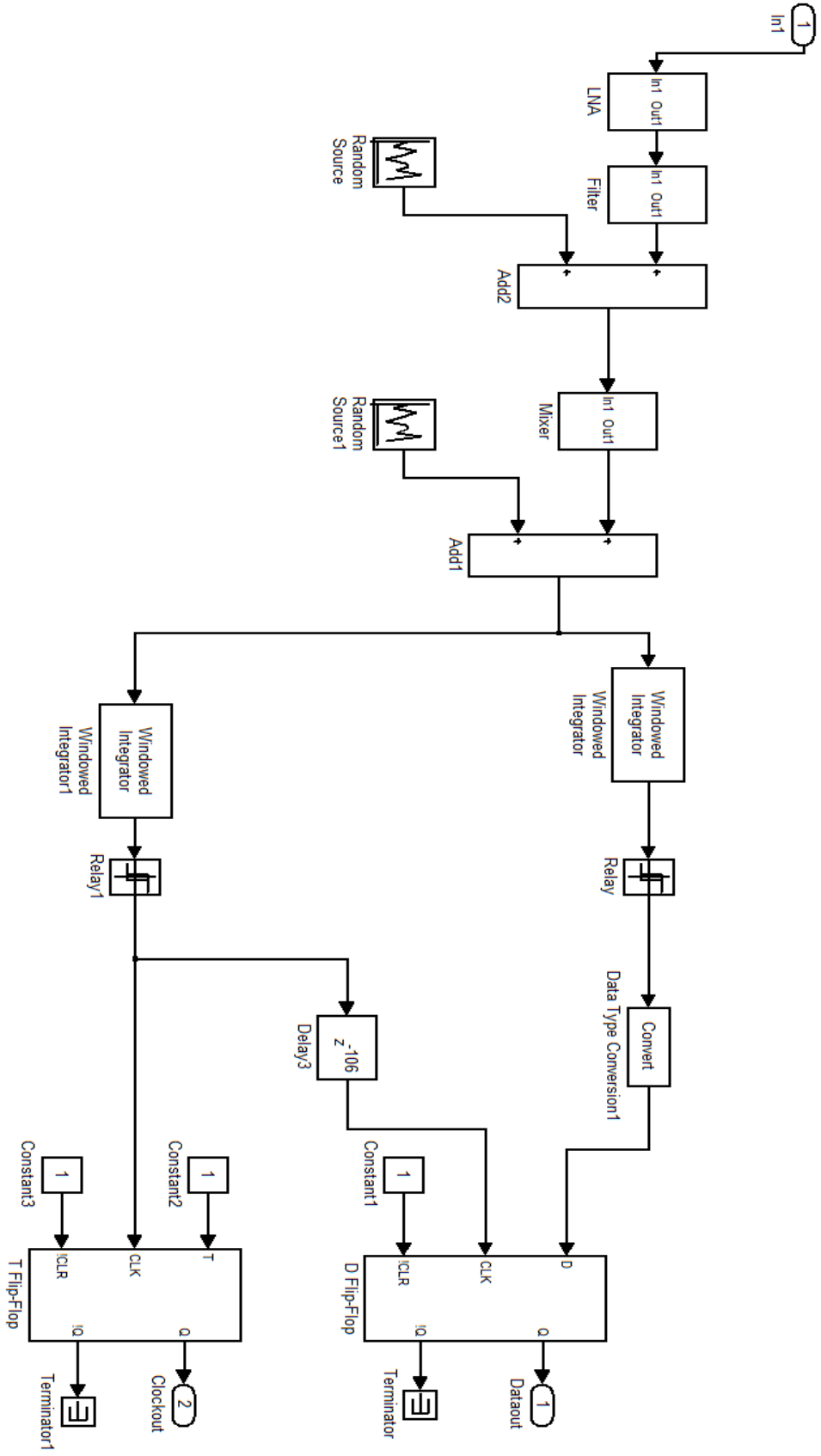

Fig.4. 38. Block diagram of the receiver

In the figure 4.38 can be seen the receiver part of the simulation platform. This simulation follows the alternative receiver solution explained before, where most of the Data transmission mode is hardware. To make the Simulink blocks like real devices and perform the simulation realistic some noise had been added. The PSD of the noise added is -174 dBm/Hz and as the figure show it is only added after the filter and the mixer. The Integrator and the Threshold also add noise in real devices but in our case the noise of these devices were not significant for the results.

In this subchapter the processes of receiver will be explained. Step by step the simulations will be shown to realize how is the course of the signal between the received signal and the recovered of the data and the clock. Depending on the step, the waveform of the signal or frequency spectrum will be used to emphasize what we want to show. At the end, the BER performance will be explained to see how the system is working with different levels of SNR.

The first step of the receiver is the LNA (Low-noise amplifier). This device is usually located after the antennas, and is used to amplify very weak signals. In our case the gain of the LNA is fixed to 12 dB, while the Noise figure is 6 dB. The figures below show the waveform and spectrum of the input and the output of the LNA.

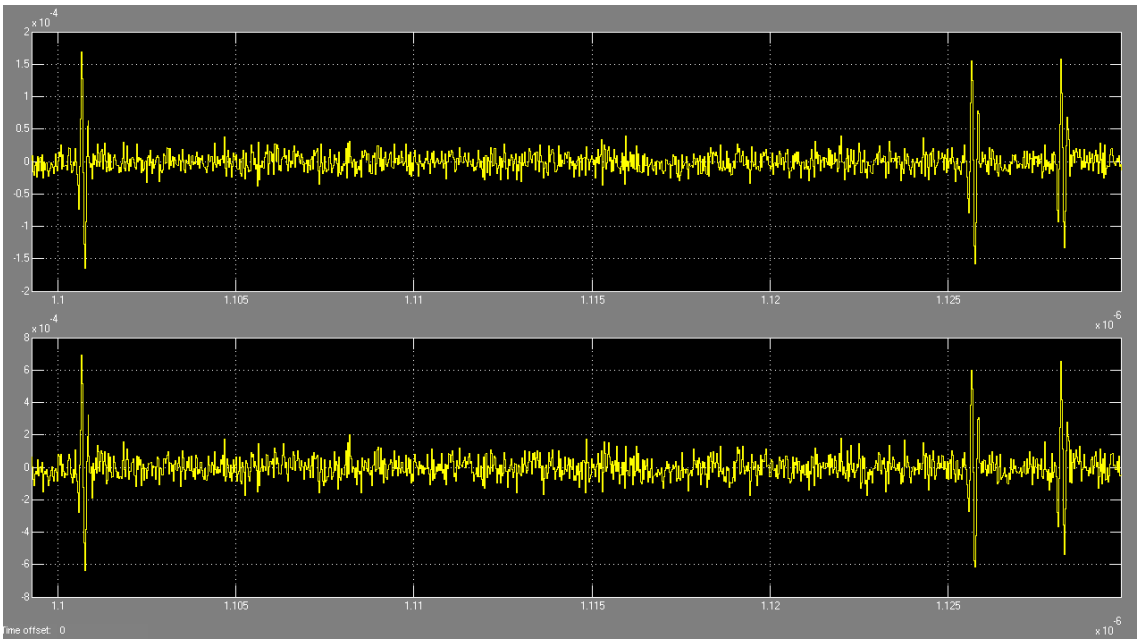

Fig.4. 39. Input and Output of the LNA in the time domain

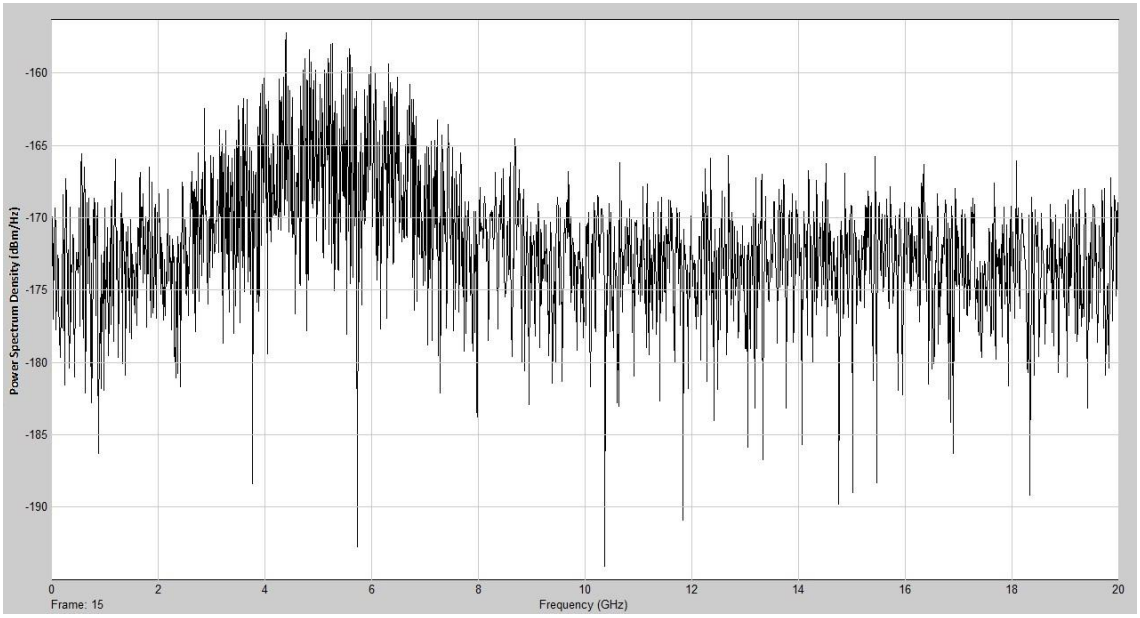

Fig.4. 40. Input of the LNA in the frequency domain

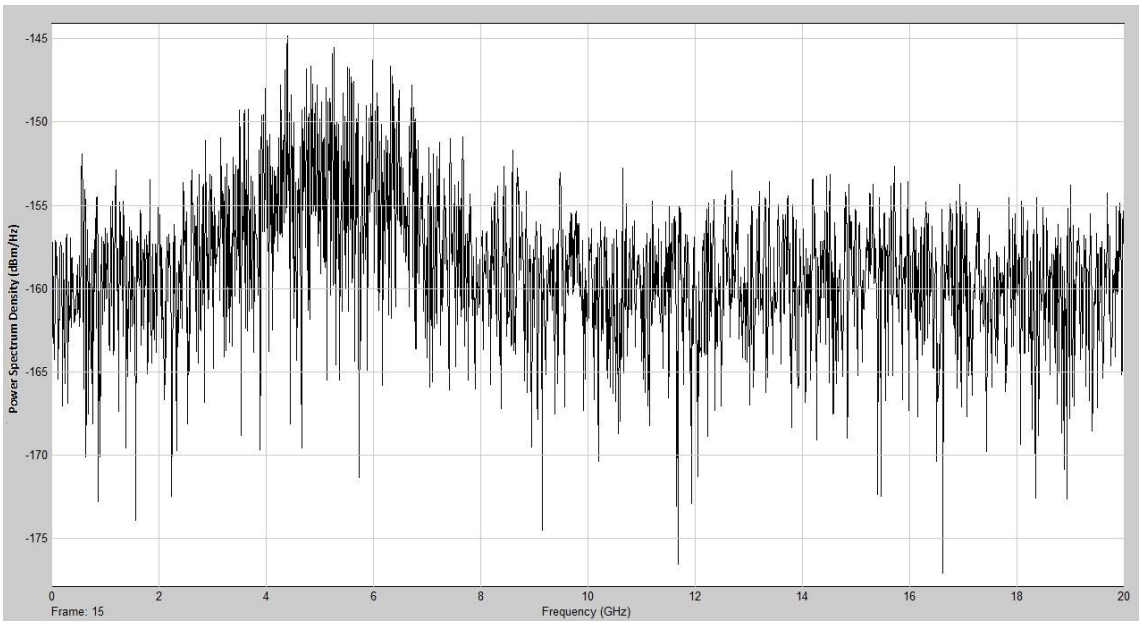

Fig.4. 41. Output of the LNA in the frequency domain

In the waveform shown in Fig.4.39 can be seen, not clearly, that the signal and noise amplitude had increase. In this case, to see how the signal had change due to the Gain and the Noise Figure of the LNA is better to see the spectrum. The signal had a power spectrum density of -165 dBm/Hz at the input (Fig.4.40) while in the output this value had increase to -153 dBm/Hz (Fig.4.41) (12 dB of Gain). About the Noise, it had increase from -174 dBm/Hz to 157 dBm/Hz (difference of aprox.17 dB due to the 12 of the Gain plus the 6 dB of the Noise Floor).

The next step of the receiver is the band pass filter (Fig.4.42). The filter was designed using the Filter design tool of Matlab. It is an IIR Butterworth filter with a band pass from 3 GHz to 8 GHz. The attenuation in the band pass is 0.5 dB.

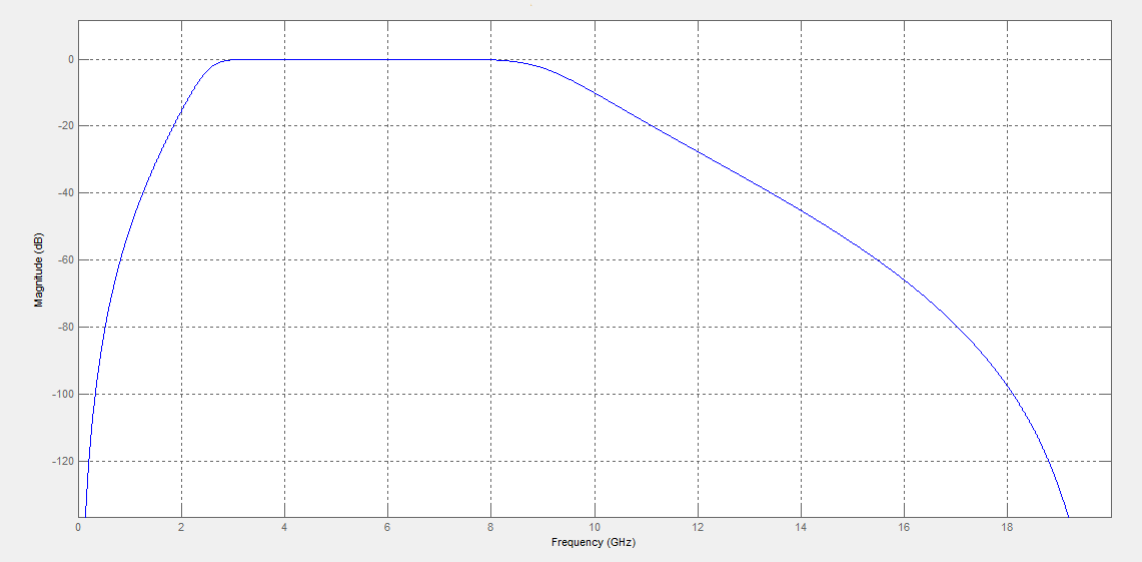

Fig.4. 42. Magnitude frequency response of the band pass filter

In the figure below can be seen the output of the BPF.

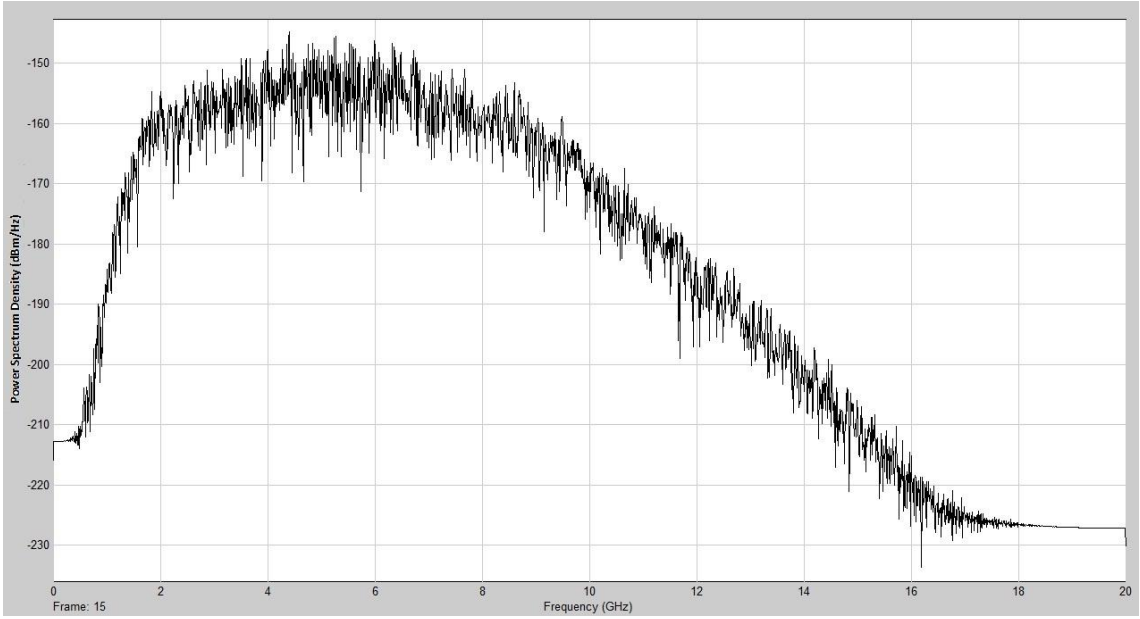

Fig.4. 43. Output of the BPF in the frequency domain

In the previous figure, it can be seen that the PSD of the noise is -220 dBm/Hz. As we want to make the simulations with real devices, this PSD of the noise is not realistic for analog devices. In the following figure the thermal noise had been added to the output of the filter.

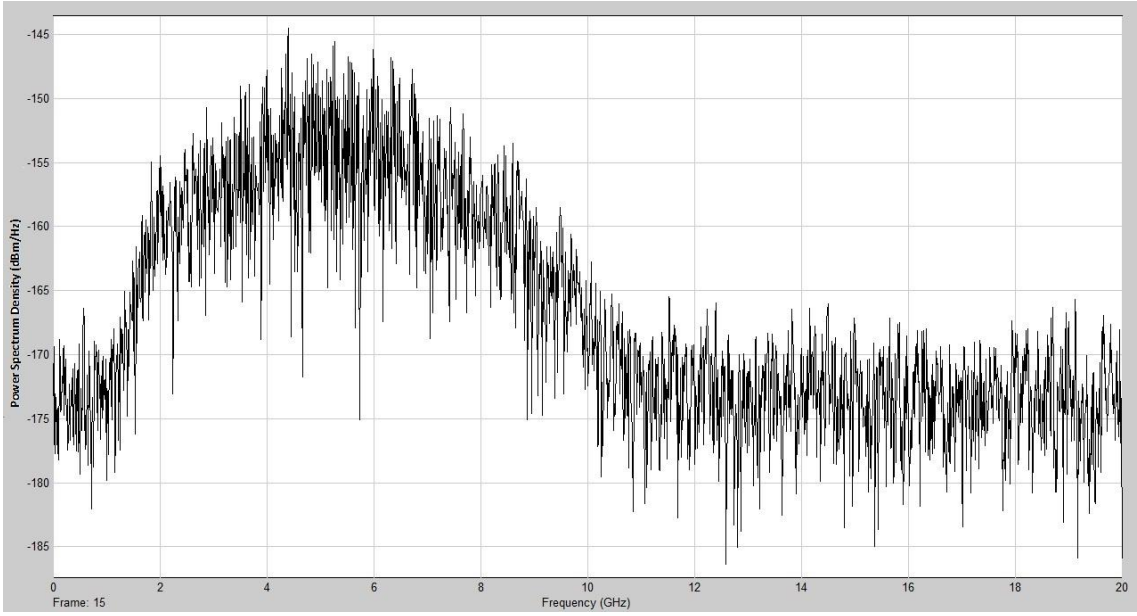

Fig.4. 44. Output of the BPF with added noise in the frequency domain

Comparing figures 4.41 and 4.44, it can be seen that the SNR of the signal had improve because the filter. In Fig.4.41 was 10 dB, while after the filter it has increase to 16 dB.

Make the square of the signal was the next of the process to design a receiver using Energy detection. In the figure below it can be seen the design of an analog mixer, which carries out with the operation of multiply the signal by itself.

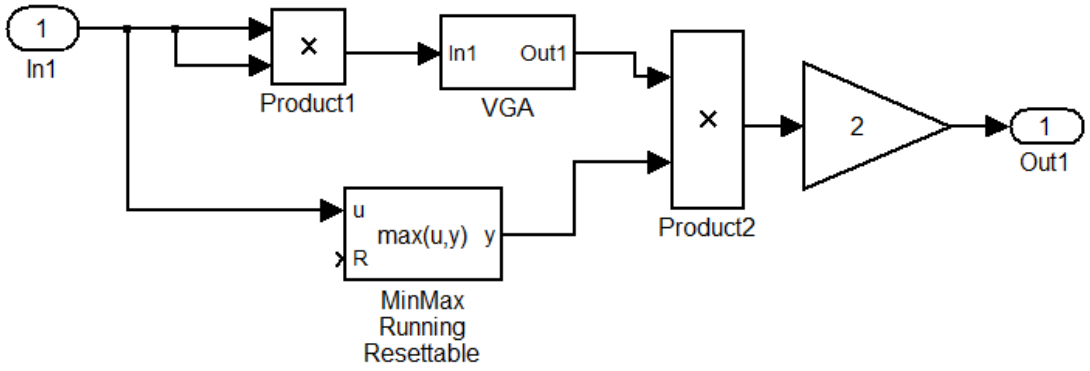

Fig.4. 45. Block diagram of the Analog Mixer

The figure shows how the analog mixer is designed. Firstly the mathematical operation of square the signal is done. Then this squared signal is normalized by the VGA (Variable Gain Amplifier). The output of the VGA is multiplied by the maximum of the signal (Maximum at the input of the Mixer). Finally the signal is multiplied by 2. All these operations are done to simulate an analog mixer.

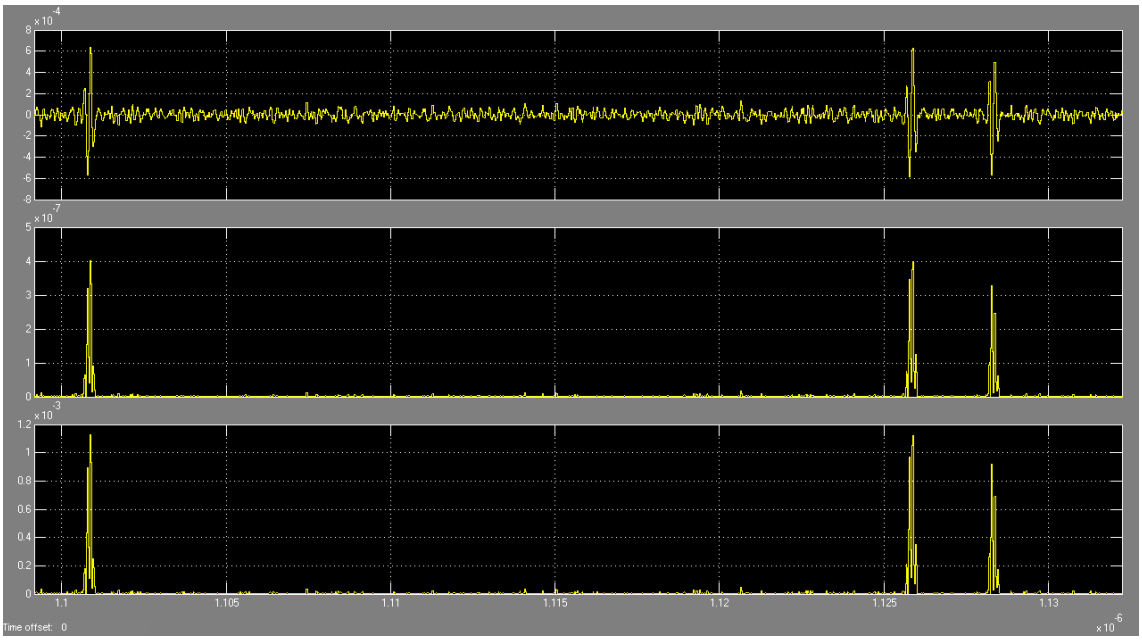

Fig.4. 46. Input of the mixer, squared signal and output of the mixer in the time domain

In the Fig 4.46, it can be seen the input of the Mixer, the signal multiplied by itself and finally the output of the Mixer. Firstly, the block that makes the mathematical operation, makes the signal positive. The other two waveforms show that the amplitude of the mixer output is higher than the amplitude of the signal squared which make it more realistic.

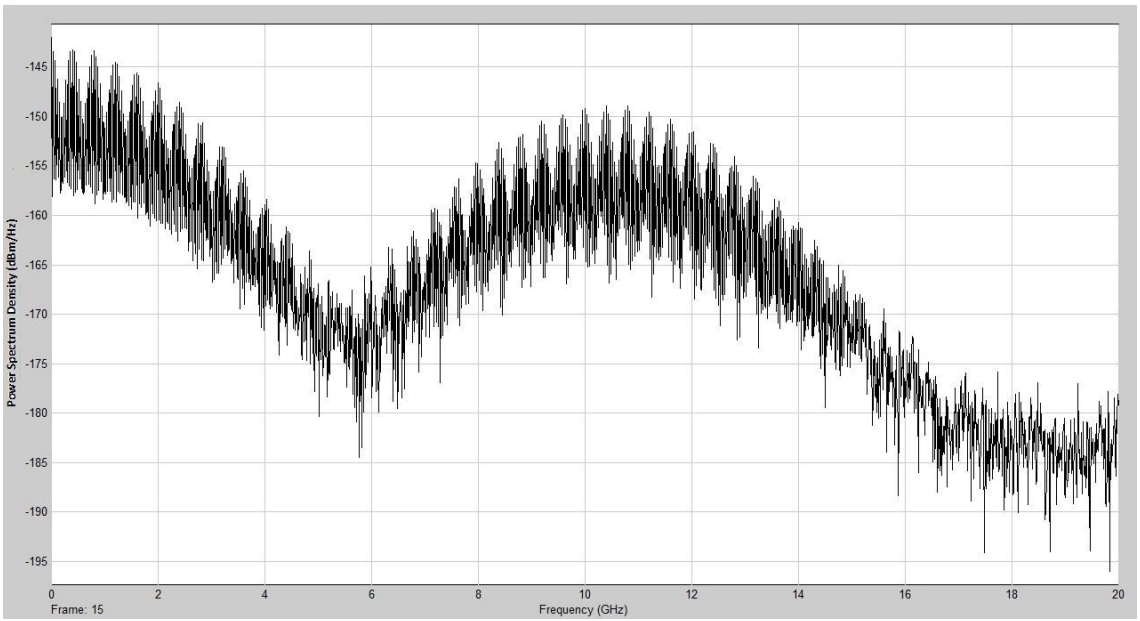

Fig.4. 47. Output of the Mixer in the frequency domain

As happened before, with the filter output, the noise PSD at the output of the mixer is too much lower because the thermal noise is not added. In the next figure is shown the output of the Mixer with the thermal noise added.

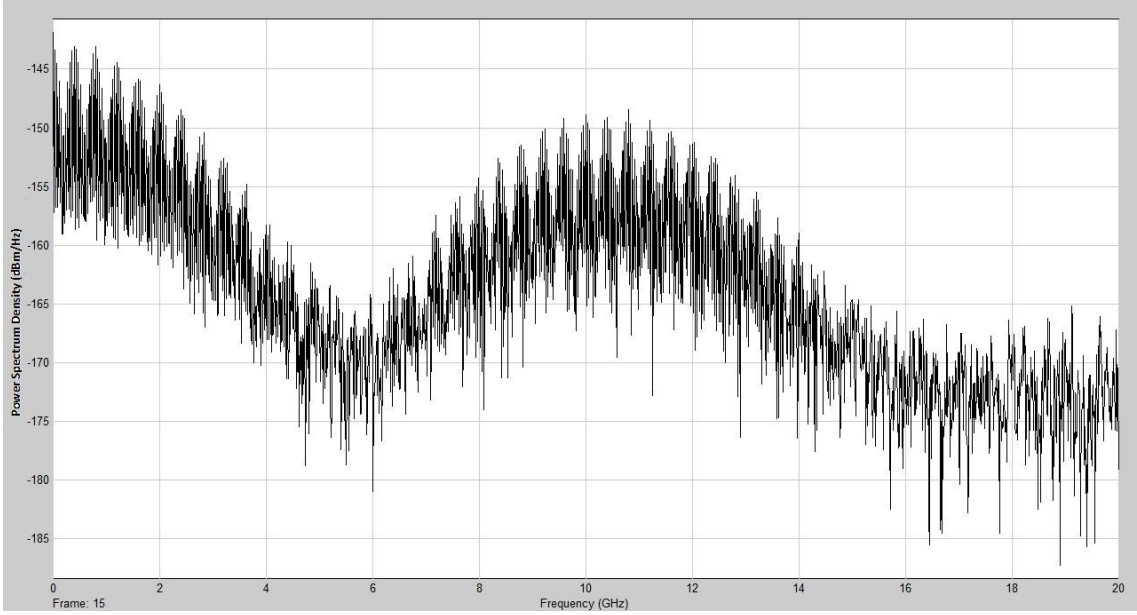

Fig.4. 48. Output of the Mixer with added Noise in the frequency domain

It can be seen in figure 4.48 that the noise PSD is -174 dBm/Hz again.

At this point the receiver is divided in two branches. One of the ramifications is used to recover the data, while the other is carried out of recovering the clock. Both branches had a windowed integrator. As is told before, the integration period is different for each case. The integration period for the data recovery is 40 samples; whilst in the branch of the clock are 200 samples. Then with different amplitudes at the output of the integrator, different thresholds had been chosen to demodulate the data and to recover the clock. As can be seen in the seconds waveforms of the figures 4.49 and 4.50, the amplitudes are $5 \cdot 10^{-3}$ V for the data branch and 0.01 V for the clock branch. Therefore the chose thresholds were $1.5 \cdot 10^{-3}$ (Switch on point) and $1 \cdot 10^{-3}$ (Switch off point) for the data, whilst in the clock the thresholds were $4 \cdot 10^{-3}$ (Switch on point) and $3 \cdot 10^{-3}$ (Switch off point).

Then in the third waveform of the figure 4.49 can be seen the pulses obtained, in this case a ‘0’ and a ‘1’ because S-OOK modulation is being used. While in the third waveform of the figure 4.50 it can be seen the pulses that while trigger the clock and data recovery.

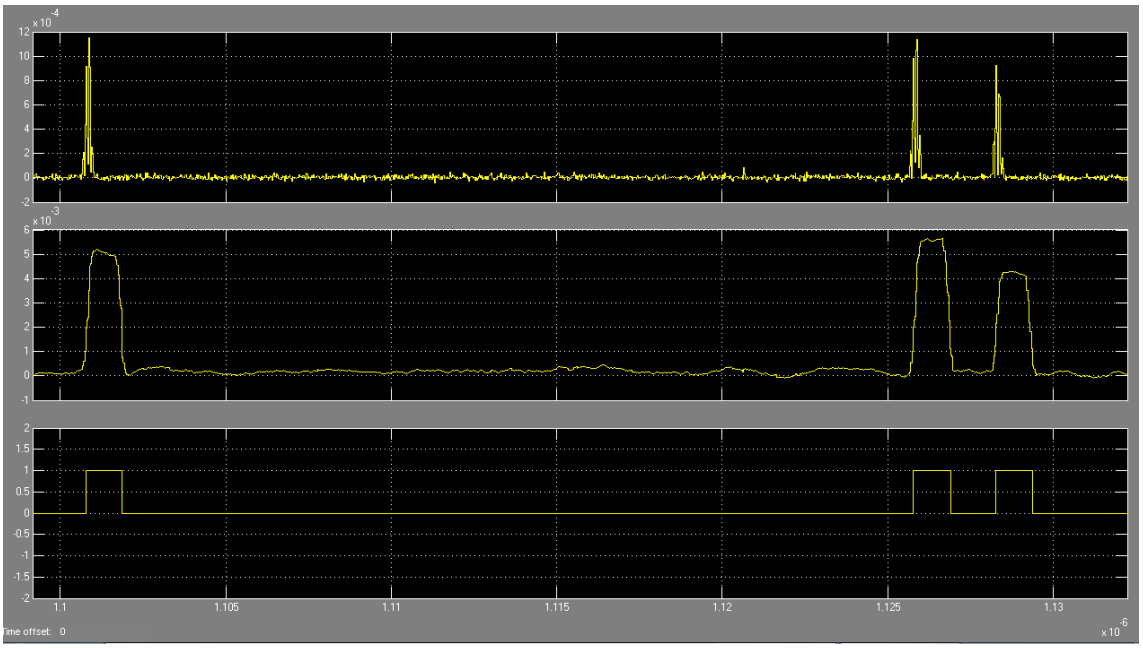

Fig.4. 49. Input and output signal of the integrator and signal after the Relay of the Data branch in time domain

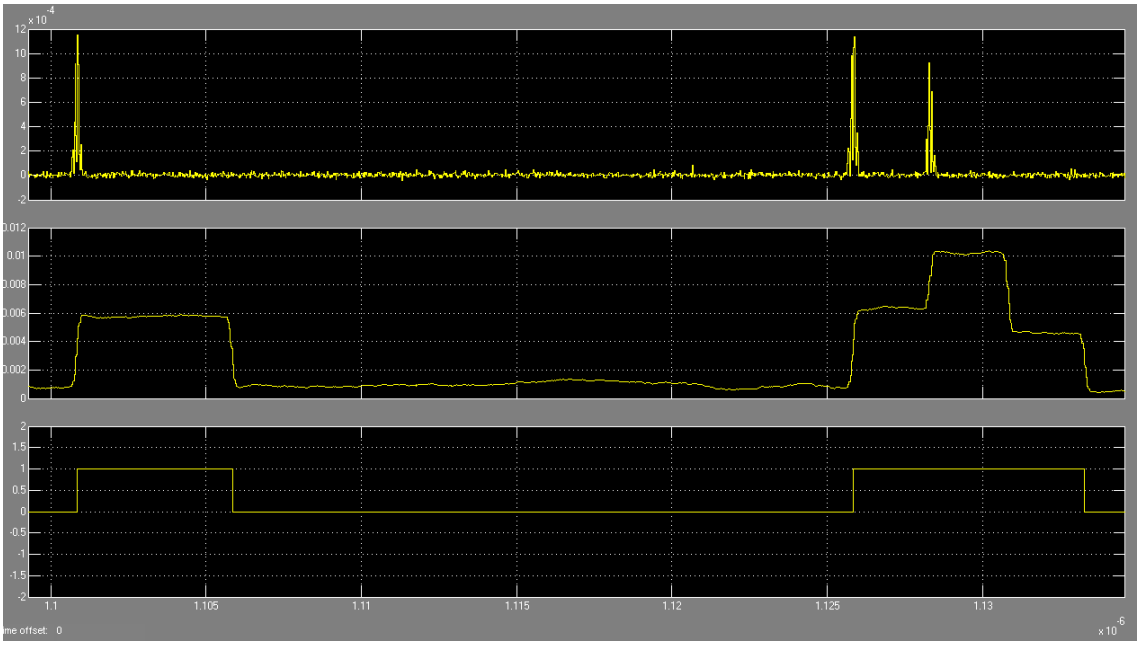

Fig.4. 50. Input and output signal of the integrator and signal after the Relay of the Clock branch in time domain

The last step of the receiver is the Flip-Flop stage. This stage is the one that demodulated the signal and recovers the clocks using the signals comings from the relays. The D-FF used is provided by Matlab, whilst the T-FF was designed by us. In the following figure can be seen the design of the T-FF.

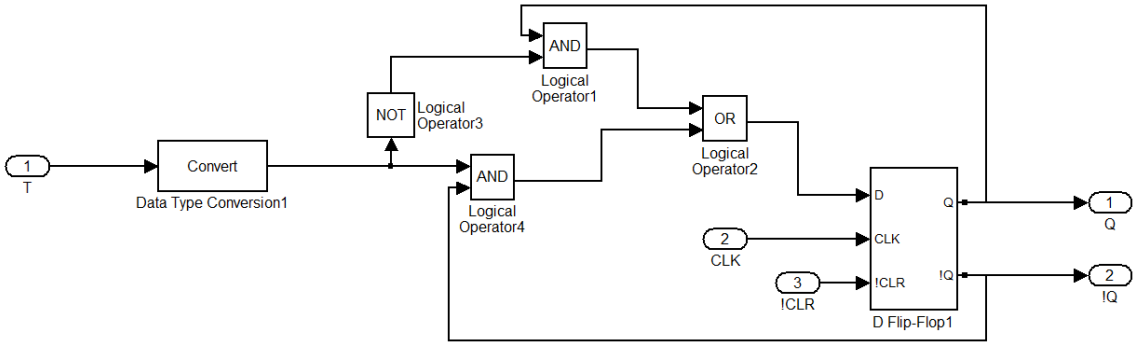

Fig.4. 51. Block diagram of the T Flip-Flop

As the figure 4.38 show, the data is demodulated using the D-FF and the clock is recovered the T-FF. Both Flip-Flops are triggered with the clock from the relay, with the only different that the D-FF trigger is delayed 106 to synchronize it with the data signal. Before the explanation of how these devices work, the truth table of both is below.

Table 4.2. Truth table of the D Flip-Flop.

D	Q	Q+
0	X	0
1	X	1

Table 4.3. Truth table of the T Flip-Flop.

T	Q	Q+
0	0	0
0	1	1
1	0	1
1	1	0

Looking the table 4.2 it can be seen that D-FF is working like a Sample and Hold. While the T-FF change the state of the Q when the input of T is ‘1’. Therefore if we fix the value of T to a constant ‘1’, this device works as an inverter every clock trigger.

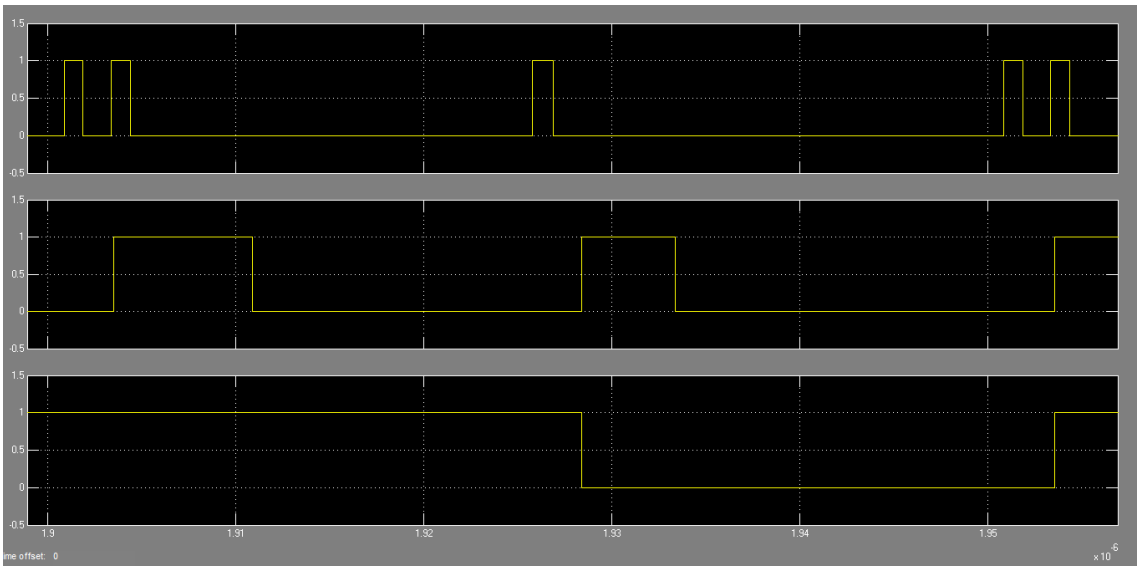

Fig.4. 52. Input of D-FF, clock and output of D-FF signals in time domain

The figure 4.52 confirms the proper functioning of the D-FF. The first waveform is the input D and the second is the clock. As is told before, when the rising edge finds a value, it is holded, while not reaching the next rising edge. The third waveform is the demodulated data, is this case a sequence of ‘1’, ‘0’, ‘1’.

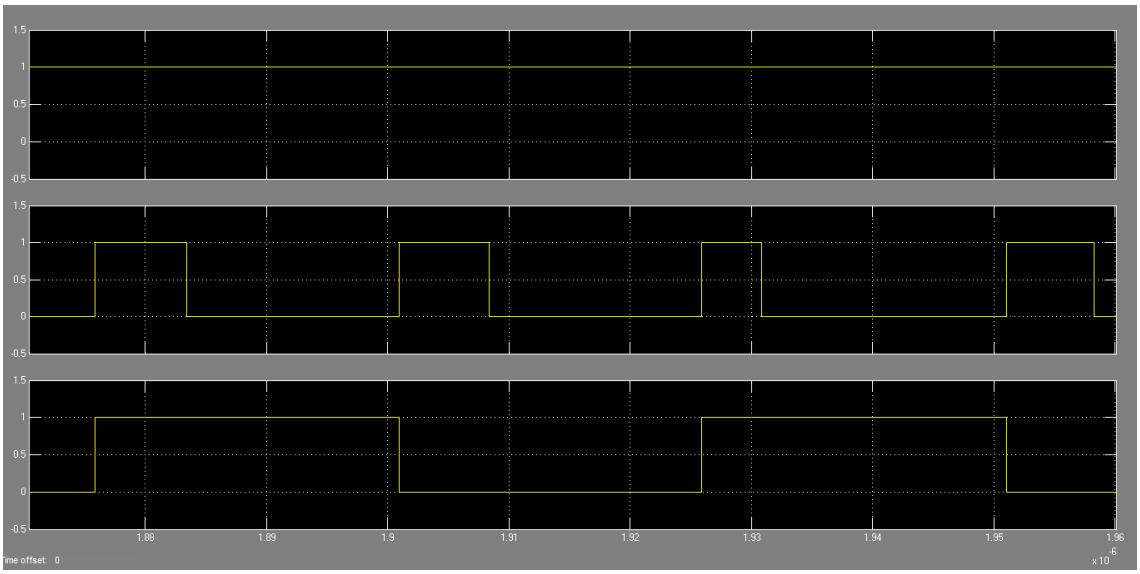

Fig.4. 53. Input of T-FF, clock and output of T-FF signals in time domain

In the figure 4.53 can be seen the functioning of the T-FF. As input T is fixed to ‘1’, the output changes every time that a Rising edge of the clock arrives. With this operation the clock is recovered.
Finally, the BER performance is shown.

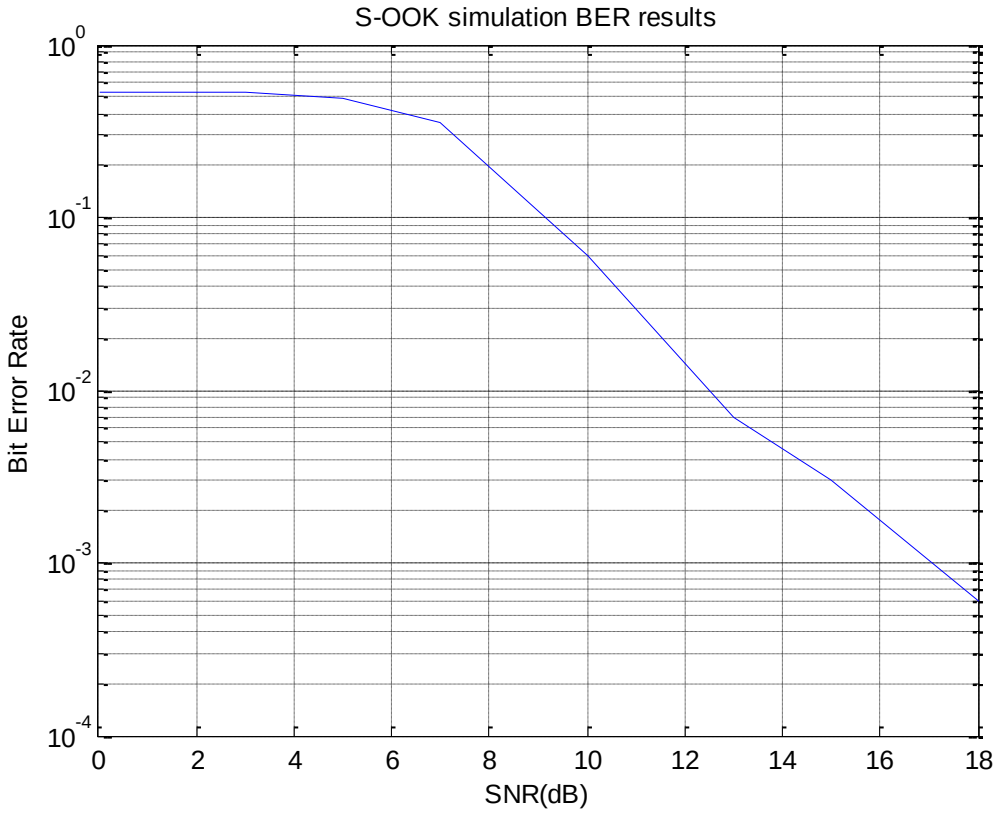

Fig.4. 54. BER vs SNR

Figure 4.54 show that between 0 dB and 6 dB the BER is close to 0.5, which can be considered a bad performance. But from this point until 18 dB of SNR a large improvement is done. It should be noted that the simulations the get BER were been done with 1000 samples from 0 dB to 17 dB and with 10000 samples in the case of 18 dB of SNR.

4.3.2. Radar mode

In the RM, the receiver must recover the signal and evaluate the time difference between the two reflected pulses. As it was said when discussing the channel modeling, the attenuation may conceal the signal in the noise. To some extent, correlating the received signal would still allow measuring the time difference between the pulses. Assuming that this time difference is known, the thickness of the medium would be obtained applying the formula 4.18, in which (Δt = = $Delay_{2T/R}$ - $Delay_{1T/R}$).

$$D_{med} = \frac{v_{med} \cdot \Delta t}{2} \quad \textbf{(4.18)}$$

CONCLUSIONS

This thesis deals with the design of a Dual-Mode Ultra-Wideband node for a RPM network. This node must be able to measure and transmit some medical parameters of a patient. The novelty of this work is that both DTM and RM are carried out with the same hardware.

Firstly, an analysis of the UWB technology and RPM systems was done. A study of the RPM present solutions showed the different technologies that can be used. A comparison with other wireless technologies, such as Wi-Fi, Bluetooth and Zigbee, was aimed at justifying the selection of this UWB among the four options. Moreover, two different types of UWB (IR-UWB and MB-OFDM UWB) were also compared to know which one of these kinds was more appropriate for our work.

Secondly, an in-depth explanation of the system and its implementation was provided. The system was divided in three main blocks: the transmitter, the channel and the receiver. Detailed explanations were given about the design and implementation of each one of these blocks.

The feasibility of the proposed platform is verified by the simulations done. Furthermore, preliminary physical experiments verified the implementation of the transmitter by showing its capability to work and switch properly between the two operation modes. Because of time and hardware resources limitations, the channel modelling and the receiver have not been validated yet.

REFERENCES

[1] World Health Organization. *World Health Statistics 2012.* Geneva, Switzerland: WHO publications, 2012.

[2] United Nations Population Found. *Population ageing and development.* New York, USA: UNPFPA, October 2002.

[3] Center for Technology and Aging. *Technologies for Remote Patient Monitoring for Older Adults.* , Oakland, USA, April 2010.

[4] Bilich, Carlos G. "Bio-Medical Sensing using Ultra Wideband Communications and Radar Technology: A Feasibility Study," in *Pervasive Health Conference and Workshops*, San Diego, USA, 2006, pp.1-9.

[5] Mathworks. "Simulink: Simulations and Model-Based design." Internet: http://www.mathworks.se/products/simulink/.

[6] Xilinx All programmable TM. "System Generator for DSP." Internet: http://www.xilinx.com/tools/sysgen.htm.

[7] Bisbe, S. "Digital platform development based in FPGA for anomalies correction in dynamic supply transistors.", TFC, Universitat Politècnica de Catalunya (UPC), Juny 2010.

[8] Reyes, C. "Development on an FPGA of a transmitter based on a LINC architecture: "Linear Amplification with Nonlinear Components"."., TFC, Universitat Politècnica de Catalunya (UPC), Juny 2010.

[9] Geozondas. *UWB Radar Evaluation Kit GZ6EVK Operation Manual.* Vilnius, Lithuania, 2009

[10] M. Shen, J.H. Mikkelsen, O.K. Jensen, T.Larsen. "Frequency Notching Applicable to CMOS Implementation of WLAN Compatible IR-UWB Pulse Generators," in *IEEE International Conference on Ultra-Wideband,* Syracuse, New York, USA, September 2012.

[11] Ministry of Health Planning and Ministry of Health Services of British Columbia. *Telehealth project: A practical Guide.*British Columbia, Canada: Ministry of Health Services, August 2001.

[12] B. Fong, A.C.M. Fong, C.K. Li. *Telemedicine Technologies.* Chichester, West Sussex, England: John Wiley & Sons Ltd, 2011.

[13] E.M. Staderini. "UWB radars in medicine," in *Aerospace and Electronic Systems Magazine,* vol. 17, pp. 13-18, January 2002.

[14] A. Aleksandrowicz, S. Leonhardt. "Wireless and Non-contact ECG Measurement System- the "Aachen SmartChair"," in *Acta Polytechnica,*vol. 47, pp. 4-5, 2007.

[15] Integrity Applications, Internet: http://www.integrity-app.com/

[16] E. Pancera, T. Zwick, W. Wiesbeck. "Ultra Wideband Radar Imaging: An Approach to Monitor the Water Accumulation in the Human Body," in *IEEE International Conference on Wireless Information Technology and Systems*, Honululu, Hawai, September 2010, pp.1-4.

[17] Deparment of Health. *Whole System Demonstrator Programme.* United States, December 2011.

[18] J.D. Taylor. *Ultra-wideband radar technology.* Danvers, Massachusetts, United States: CRC Press LLC, 2001.

[19] F. Ramírez-Mireles. "Una introducción a IR-UWB con resultados de investigacions." Internet: http://www.slideshare.net/ETSITUPV/una-introduccin-a-iruwb-con-resultados-de-investigacin.

[20] V. Lakkundi. "Ultra Wideband Communications: History, Evolution and Emergence"," in *Acta Polytechnica,*vol. 46, 2006.

[21] Radio-Electronics.com. "Multiband OFDM UWB." Internet: http://www.radio-electronics.com/info/wireless/uwb/mb-ofdm-uwb.php.

[22] M.Shen. "*Low Power UWB System and Circuits Designs for Wireless Sensor Networks,*" Department of Electronic Systems, Aalborg University, Denmark, January 2012.

[23] M.Crepaldi, C.Li, J.R.Fernandes and P.R.Kinget. "An Ultra-Wideband Impulse-Radio Transceiver Chipset Using Synchronized-OOK Modulation," *IEEE Journal of Solid-State circuits*, vol. 46, pp. 2284-2299, October 2011.

[24] I.Oppermann, M.Hamalainen and J.Iinatti. *UWB Theory and applications*. Chichester, West Sussex, England: John Wiley & Sons Ltd, 2004.

[25] X. Chen, S. Kiaei. "Monocycle shapes for Ultra Wideband System," *IEEE Sympsosium on Circuits and Systems,* vol. 1, pp. I-597 - I-600, 2002.

[26] L. Niestoruk, O. Perkuhn, W. Stork. "The experimental results of tissue thickness estimation with UWB signals for the purpose of detecting water accumulations in the human body," in *10th International Workshop on Biomedical Engineering,* pp. 1-4, October 2011.

[27] A.Muqaibel, A. Safaai-Jazi, A.M. Attiva, S.M. Riad, A. Bayram. "Through-the-Wall Propagation and Material Characterization," in *IEEE Proceedings-Microwaves, Antennas and Propagation,* pp. 581-588, December 2005.

[28] A. Lonappan, V. Hamsakkuty, G. Bindu, J. Jacob, V. Thomas, K.T. Mathew. " Dieletric properties of human urine at microwave frequencies," of Department of Electronics, Microwave Tomography and Materials Research Laboratory, Cochin University, India, March 2004.

[29] C. Gabriel, S. Gabriel, and E. Corthout. “The dielectric properties of biological tissues I: Literature survey,” in *Physics in Medicine and Biololgy*, vol. 41, pp. 2231–2249, 1996.

[30] S. Gabriel, R.W. Lau, and C. Gabriel, “The dielectric properties of biological tissues II: Measurements on the frequency range 10 Hz to 20 GHz (literature survey),” in *Physics in Medicine and Biololgy,* vol. 41, pp. 2251–2269, 1996.

[31] S. Gabriel, R.W. Lau, and C. Gabriel, “The dielectric properties of biological tissues III:Parametric models for the dialectic spectrum of tissues ” in *Physics in Medicine and Biololgy,* vol. 41, pp. 2271–2293, 1996.

[32] L. Stoica. “Non-coherent energy detection transceivers for Ultra Wideband Impulse Radio Systems.” Thesis, University of Oulu, Finland, February 2008.

[33] B&K Precision Corporation. “Understanding Real Time and Equivalent Time Sampling.” Internet: http://kb.bkprecision.com/questions.php?questionid=227.

[34] C.Chen, S.Wu, S.Meng, J.Chen, G. Fang, H. Yin. “Application of Equivalent-time Sampling Combined with Real-time Sampling in UWB Through-wall Imaging Radar” in *International Conference on Instrumentation, Measurement, Computer, Communication and Control,* 2011.